

Article

Catalytic Etching and Oxidation of Platinum Group Metals: Morphology, Chemical Composition and Structure of Pt, Pd and Rh Foils in the O₂ Atmosphere and during NH₃ Oxidation with Air at 1133 K

Aleksei Salanov *, Alexandra Serkova, Lyubov Isupova , Sergey Tsybulya and Valentin Parmon

Boriskov Institute of Catalysis SB RAS, 630090 Novosibirsk, Russia

* Correspondence: salanov@catalysis.ru

Abstract: Platinum alloy gauzes are employed for the high-temperature oxidation of NH₃ to NO used in the industrial production of HNO₃ for application in agricultural fertilizers. To enhance the efficiency of NH₃ oxidation, various Pt–Pd–Rh alloys are employed for the production of such catalytic gauzes. To understand the role of these metals in NH₃ oxidation, scanning electron microscopy, energy-dispersive spectroscopy and X-ray diffraction were applied to investigate the morphology, composition and structure of Pt, Pd and Rh foils after annealing in O₂ and oxidation of NH₃ with air at 1133 K. After annealing in O₂ and NH₃ oxidation, the metallic microgranular structure was detected on Pt(poly), whereas oxide layers of Rh₂O₃ and PdO were observed on Rh(poly) and Pd(poly). At the onset of NH₃ oxidation (*t* = 1 h), fibrous metal-oxide agglomerates of nanofibers formed on these oxide layers. The long-term (5–10 h) oxidation of NH₃ led to the formation of a continuous layer of pyramidal crystals on Rh(poly) and palladium “cauliflowers” on Pd(poly). The highly exothermic reaction of NH₃ with oxygen on metals and PdO or Rh₂O₃ initiates strong catalytic etching forming grains and facets on Pt, fibrous metal-oxide agglomerates, pyramidal crystals and metallic “cauliflowers” on Rh and Pd.

Keywords: ammonia oxidation; platinum group metals; metal oxidation; catalytic etching; morphology; chemical composition



Citation: Salanov, A.; Serkova, A.; Isupova, L.; Tsybulya, S.; Parmon, V. Catalytic Etching and Oxidation of Platinum Group Metals: Morphology, Chemical Composition and Structure of Pt, Pd and Rh Foils in the O₂ Atmosphere and during NH₃ Oxidation with Air at 1133 K. *Catalysts* **2023**, *13*, 249. <https://doi.org/10.3390/catal13020249>

Academic Editors: Alessia Ciogli and Antonia Iazzetti

Received: 8 December 2022

Revised: 13 January 2023

Accepted: 16 January 2023

Published: 21 January 2023



Copyright: © 2023 by the authors. Licensee MDPI, Basel, Switzerland. This article is an open access article distributed under the terms and conditions of the Creative Commons Attribution (CC BY) license (<https://creativecommons.org/licenses/by/4.0/>).

1. Introduction

Owing to their unique properties, including high chemical and etching resistance, stability at high temperatures, catalytic activity, etc., platinum group metals (PGMs) are widely used in various spheres of human activity [1,2]. PGMs are applied on a large scale to produce autocatalysts intended for the neutralization of hazardous CO, C_xH_y and NO_x emissions from automotive internal combustion engines. In 2021, ca. 71% of Pt, Pd and Rh produced in the world was used for the synthesis of autocatalysts [1,2]. PGMs are also employed to obtain catalysts that serve in the chemical industry for manufacturing various organic and inorganic chemicals and in the environmental protection for remediation of industrial wastes. In addition, PGMs are used in other fields, particularly in fuel cell technologies, hydrogen energetics, medicine, electronics, jewelry production, etc. [1]. Pt, Pd and Rh are used to obtain alloys that are employed in the production of metal gauze catalysts. Platinum alloy gauzes with the predominant content of platinum are applied in the industrial high-temperature oxidation of ammonia with air oxygen to nitrogen oxide NO, which is used to produce nitric acid [3–5].

The world’s annual production of HNO₃ reaches 70–80 million tons. Nearly 80% of the produced acid is consumed to manufacture agricultural fertilizers. The application of Pt–Rh and Pt–Pd–Rh alloys increases the activity and enhances the performance of catalytic gauzes in the high-temperature NH₃ oxidation compared to gauzes made of neat Pt [5,6].

Efforts are now made to find new ways to enhance the efficiency of catalysts intended for the industrial high-temperature oxidation of NH_3 to NO [7,8]. This can be achieved by revealing the effect of various factors, particularly the type of gauze (woven, knitted, etc.), different metals, their binary and ternary alloys, as well as their oxidation and etching, on the efficiency of NH_3 oxidation catalysts [7,8].

Surface etching of Pt, Rh, Pd, Ag, Ir and Pt–Rh, Pt–Ir, Pd–Ni alloys and transfer of the metals are strongly affected by the reaction medium, temperature and catalyst composition [9–13]. For neat Pt and Rh in the atmosphere of O_2 , air, H_2O vapor or under vacuum, the transfer of Pt(Rh) metals was equal to 193(2), 43(4), 1(6) and 3(2) μg , respectively [9]. The surface morphology of the wire made of Pt, Rh and Pt/10–30 wt.% Rh substantially depends on the temperature upon treatment with O_2 , N_2O and NO flows [10]. After treatment of such a wire in O_2 ($P_{\text{O}_2} \approx 1$ bar) for 72 h, grain boundaries, facets, etch pits, and small crystals were detected on the wire surface. For neat Pt and Pt/10 wt.% Rh alloy, etch pits concentrated mostly in the central part of the wire, where the temperature reached a maximum (ca. 1173 K), while crystals grouped at the wire ends with the minimum temperature (≤ 973 K). For rhodium-containing alloys, the surface enrichment with rhodium and the appearance of Rh_2O_3 crystals were observed, while for neat Rh, the formation of a continuous Rh_2O_3 oxide layer. The revealed mass transfer of metals and surface rearrangement for neat Pt, Rh and Pt alloys with different Rh content during treatment of the samples by individual reagents (O_2 , air, H_2O , vacuum, NO , N_2O , etc.) can be associated with the transport of $\text{PtO}_2(\text{gas})$ and $\text{RhO}_2(\text{gas})$, which are formed on hot surface regions, to cold surface regions of metals and their alloys by the Chemical Vapor Transport (CVT) mechanism [9,10]. Oxygen and other reagents initiate the transfer of metals and the surface reconstruction of metals and their alloys [9,10]; however, upon NH_3 oxidation with oxygen, the mass transfer proceeds much more intensely and results in deeper structural rearrangement of the catalysts' surface [11–13].

The data reported in [11–13] showed a strong dependence of the surface etching on the catalyst composition for the wire sections that were used in NH_3 oxidation, had a diameter of 0.2 mm and length of ca. 100 mm and consisted of neat metals Pt, Rh, Pd, Ag, Ir, Au and alloys Pt/5–40 wt.% Rh, Pt/10–20 wt.% Ir and Pd/5 wt.% Ni. For all the tested materials, three main regions with different morphology and temperature were distinguished on the wire along the gas flow. The region indicating the onset of NH_3 oxidation and surface etching processes was located at a distance of 1–(2–6) mm from the inlet of the reaction mixture to the reactor. This region had a low temperature (< 1173 K) and minor changes in the surface morphology. The main reaction zone of NH_3 oxidation, characterized by a high temperature (ca. 1173 K) and strongly etched surface with “cauliflowers”, was detected at a distance of (2–6)–(20–85) mm. Outside the reaction zone of (20–85)–100 mm, the region with a lower temperature (< 1173 K) and generally a smooth surface was observed. After NH_3 oxidation for 386 h on Pt, terraces 5–10 μm in width with hollows 0.1–0.5 μm in diameter were detected at a distance of 1–2 mm from the front end of the wire [11]. As the distance from the wire front end was increased (≥ 2 mm), extended facet-like crystal structures ca. 1 μm in height appeared on the surface, while crystal Pt “cauliflower” agglomerates with the size of 5–20 μm appeared in the main reaction zone at a distance from 4 to 40 mm. A further increase in the distance from the wire front end (> 40 mm) was accompanied by a decrease in the size of facets and “cauliflowers”; this led to the gradual formation of terraces, which resemble those obtained at the wire front end.

After NH_3 oxidation for 23 h on Rh, deep grain boundaries with large cracks were found at a distance of 1–3 mm from the wire front end [12]. In the main reaction zone, at a distance of 3–70 mm, “cauliflowers” with the size of ca. 3–16 μm were detected. At a distance of 60–70 mm, sizes of “cauliflowers” grew to 80 μm . Outside the reaction zone, at a distance of > 70 mm, a smooth surface with the fibrous structure on Rh was seen. In addition, for Rh, Rh_2O_3 whiskers were found on the surface of “cauliflowers” at a distance of 60–70 mm, while “wool”-like deposits of Rh_2O_3 were observed on a smooth surface at a distance > 70 mm. These oxide structures were detected outside the main reaction zone of NH_3 oxidation (≥ 60 –70 mm) in the low-temperature region. It should be noted

that the oxidation of NH_3 on Rh was accompanied by uncontrolled temperature elevation above 1173 K due to intense oxidation of NH_3 , and mechanical destruction of the wire was observed after 60 h. After NH_3 oxidation for 54 h on Pd, terraces, facets and etch pits were detected on the surface at a distance of 1–2 mm from the wire front end [13]. In the main reaction zone (2–20 mm), palladium “cauliflowers” with the size of 4–30 μm were found at 2–4 mm, while larger “cauliflowers” (20–55 μm) were seen at 4–20 mm. Outside the reaction zone, at 20–30 mm, the Pd surface was covered with “wool”-like deposits of PdO, while at 30–100 mm, a continuous PdO oxide layer with a thickness of ca. 4 μm was observed. This testifies to the decomposition of PdO oxide at a high temperature in the reaction zone (2–20 mm) and the formation of this oxide at low temperatures outside this zone. It should be noted that NH_3 oxidation on Pd for 54 h was followed by mechanical destruction of the wire, which could occur due to intense oxidation of NH_3 leading to uncontrolled elevation of temperature above 1173 K. Data reported in [11–13] testify to a strong effect of both the catalyst composition and temperature on the catalyst etching.

Data concerning the effect of Pt, Pd and Rh metals on the catalytic etching initiated by the high-temperature oxidation of ammonia are reported only in a few publications, which do not allow the role of these metals in the etching process to be revealed. Generally, the data concerning the deep etched layers formed after long-term oxidation of NH_3 ($t \geq 20$ –50 h) are reported. In this connection, the onset of the etching process, including the nucleation and growth of etching structures, is usually not detected. In addition, the literature does not provide data on the effect exerted by the oxidation of these metals on the surface rearrangement during NH_3 oxidation, which also makes it difficult to elucidate the mechanism of catalytic etching. Our earlier publications [14–19] contain data on the morphology and chemical composition of the rough surface layer, which is formed upon catalytic etching of Pt–Pd–Rh–Ru gauzes initiated by the long-term (50 h) oxidation of NH_3 .

In this paper, we describe our results on the oxidation and etching of Pt, Pd and Rh polycrystalline foils (Pt(poly), Pd(poly) and Rh(poly)) after annealing in the O_2 atmosphere and NH_3 oxidation with air at ca. 1100 K for $t \leq 10$ h. This allowed us to analyze the initial step of the etching process and obtain important results concerning the nucleation mechanism of etching structures. The study was performed using scanning electron microscopy (SEM), energy-dispersive X-ray spectroscopy (EDS) and X-ray diffraction (XRD) [20,21]. The study aimed to obtain new data on the morphology, composition and structure of the etched layers formed upon annealing in O_2 and NH_3 oxidation on Pt, Pd and Rh at the beginning of the etching process (for $t \leq 10$ h). Particular attention was paid to revealing the role of these metals and their oxidation in the nucleation and growth of etching structures during NH_3 oxidation. The data obtained made it possible to comprehensively analyze the process of catalytic etching on Pt alloy gauzes initiated by the oxidation of NH_3 .

2. Results

2.1. Morphology and Chemical Composition of the New Pt(poly), Pd(poly) and Rh(poly) Samples

Figure 1 displays SEM images and EDS spectra for the new samples Pt(poly) (a,b), Pd(poly) (c,d) and Rh(poly) (e,f) after purification of the surface by treatment in nitric acid and distilled water. The images were obtained in SE mode at $E_0 = 20$ keV and a $\times 1000$ magnification. They show mostly a smooth surface of the samples with the rolling traces represented by hollows, protrusions and extended strips with a predominant size ≤ 1 μm . EDS spectra were recorded at a probe electron energy $E_0 = 20$ keV and the energy of X-ray quanta (E) 0–10.0 keV on the regions with the size of 20×20 μm . Figure 1b,d,f displays fragments of these EDS spectra in the energy range of 0–4.0 keV, which contains the main recorded X-ray peaks for C and O (K series) and for Pt, Pd and Rh (M and L series). On Pt(poly), the X-ray peaks for Pt were obtained at $E = 1.59$ – 2.69 keV (M series) and $E > 8.27$ keV (L series), while the peaks for C and O were obtained at $E = 0.277$ and 0.526 keV, as shown in Figure 1b. For Pt(poly), the concentration of Pt, C and O appeared equal to 71.1, 28.2 and 0.7 at.%. On Pd(poly), the X-ray peaks were obtained for Pd at $E = 0.28$ – 0.56 keV (M series) and 2.5 – 3.55 keV (L series), as well as the peak for C,

as shown in Figure 1d. The concentrations of Pd and C were equal to 82.1 and 17.9 at.%. On Rh(poly), the X-ray peaks for Rh were obtained at $E = 0.26\text{--}0.50$ keV (*M* series) and $2.38\text{--}3.36$ keV (*L* series), as shown in Figure 1f. On Rh(poly), the concentrations of Rh, C and O constituted 62.1, 30.6 and 7.3 at.%. It should be noted that Fe impurities detected in the concentration from 0.1 to 0.3 at.% on some regions of this sample may belong to the initial metal.

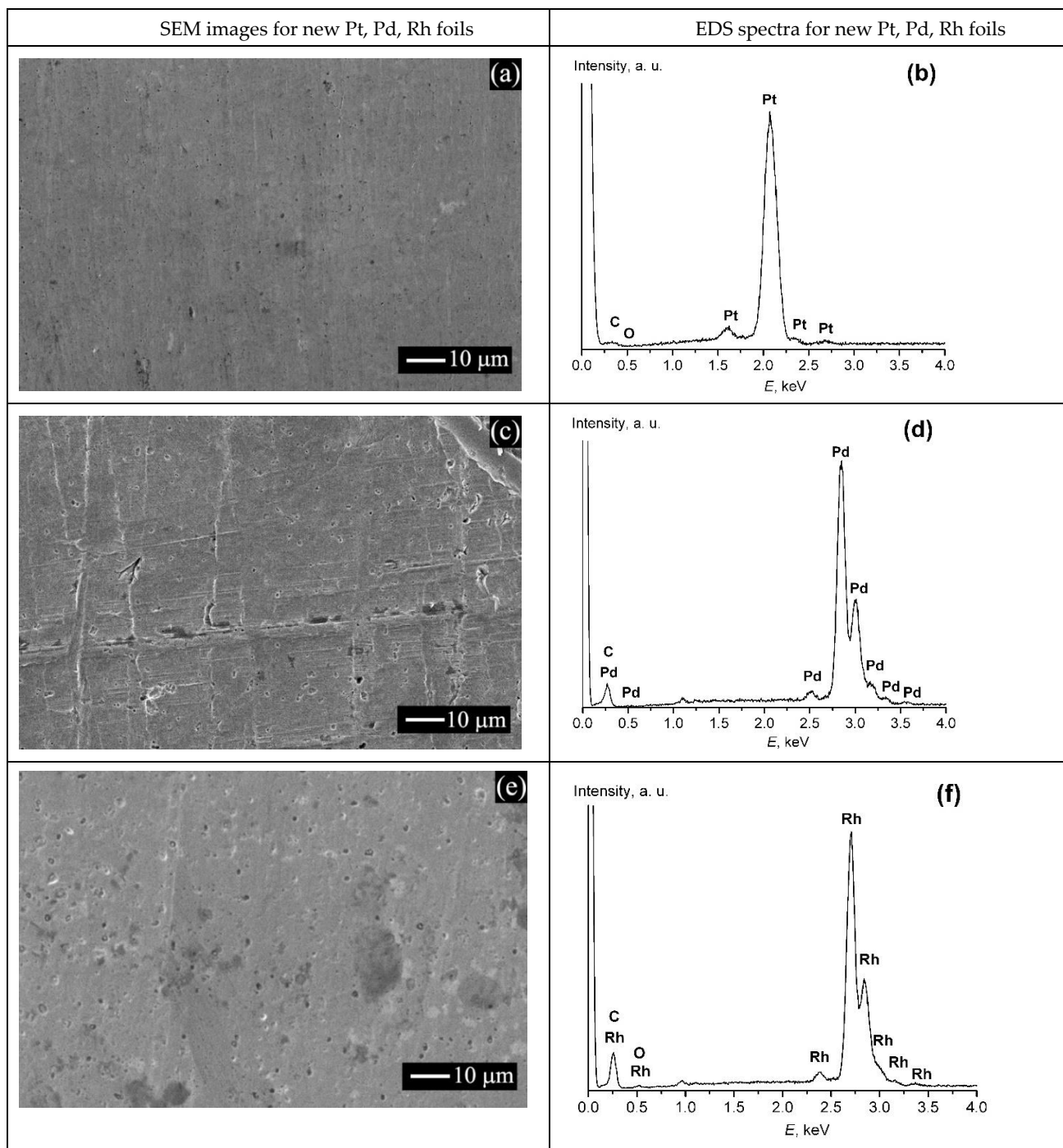


Figure 1. SEM images and EDS spectra for the new samples Pt(poly) (a,b), Pd(poly) (c,d) and Rh(poly) (e,f). Images were obtained in SE mode at $E_0 = 20$ keV and a $\times 1000$ magnification. The EDS spectra in the energy range from 0 to 4.0 keV were recorded at $E_0 = 20$ keV and the energy of X-ray quanta 0–10.0 keV.

According to EDS data, the new samples Pt(poly), Pd(poly) and Rh(poly) contain, in addition to metals, only C and O impurities; other impurities are not detected. It should

be noted that the detection limit of elements for standard EDS analysis is ca. 0.1 wt.%. Therefore, it is impossible to detect the impurity elements that could be present in the metals according to GOST 13498-2010, 13462-2010 and 13098-2006 in the concentration ≤ 0.1 wt.%. In addition, according to these GOSTs, the above-listed impurities can be absent in the metals (see below Section 4).

Note that at the temperature of the samples (ca. 1100 K) used in this study, metal atoms can migrate both over the surface and in bulk during the oxidation of metals and catalytic oxidation of NH_3 . Mobility of the atoms increases with an elevation of the temperature, thus accelerating the recrystallization processes, which include the disappearance of various defects, grain nucleation and growth, as well as a faceting of the grain surface with different faces. The mobility of metal atoms at a temperature T K is estimated from the T/T_{melt} value, where T_{melt} is the melting point of a metal. For Rh, Pt and Pd, T_{melt} is equal to 2239, 2042 and 1825 K, respectively. It is commonly accepted that at $T/T_{\text{melt}} \leq 0.3$, metal atoms have a low mobility, which increases considerably when the Tamman temperature (T), for which $T/T_{\text{melt}} \sim 0.5$ or $T/T_{\text{melt}} > 0.5$, is reached. It should be noted that the Tamman temperature for Rh, Pt and Pd has the values of 1119.5, 1021.0 and 912.5 K, respectively. Hence, at the temperature used in this study (ca. 1100 K), atoms of the indicated metals will be highly mobile.

2.2. Morphology and Chemical Composition of Pt(poly), Pd(poly) and Rh(poly) in the O_2 Atmosphere

X-ray photoelectron spectroscopy (XPS), XRD, SEM and EDS methods allowed us to reveal an essential effect of the treatment temperature in the O_2 atmosphere on the morphology, microstructure and chemical composition of the surface and subsurface layers of Pt(poly) [21]. The noticeable dissolution of oxygen in the platinum lattice and the formation of particles and/or crystals of bulk oxide like $\text{PtO}_2(\text{solid})$ were not detected; however, we observed the accumulation of oxygen atoms on the platinum surface and grain boundaries in the concentration of 5–10 at.%. Figure 2a shows the concentrations of oxygen estimated by EDS after treatment of the samples in O_2 at temperatures from 600 to 1400 K for 3 h, for Pt(poly) (1) at $P_{\text{O}_2} = 2.1 \times 10^4$ Pa, and for Pd(poly) (2), Rh(poly) (3)—at $P_{\text{O}_2} = 10^5$ Pa. The dependence for Pt(poly) (1) was reported earlier in [21]. As the temperature is increased from 600 to 1400 K, a minor decrease in the oxygen concentration from 10.0 to 7.0 at.% is observed for Pt(poly), whereas for Pd(poly) and Rh(poly) this value grows significantly to 33.0 and 69.1 at.% at 1400 K, respectively. Low concentrations of O atoms for Pt(poly) are related to the absence of both the dissolution of O atoms in the Pt lattice and the formation of PtO_2 solid oxide particles, whereas the dissolution of O atoms in the lattice of Pd and Rh and the formation of particles and/or crystals of PdO and Rh_2O_3 solid oxides lead to high oxygen concentrations on these metals.

Figure 2b displays temperature dependencies of the equilibrium O_2 pressure for solid oxides PtO_2 (1), PdO (2) and Rh_2O_3 (3), which dissociate by the reactions $\text{PtO}_2(\text{solid}) = \text{Pt}(\text{solid}) + \text{O}_2(\text{gas})$, $2\text{PdO}(\text{solid}) = 2\text{Pd}(\text{solid}) + \text{O}_2(\text{gas})$ and $2/3\text{Rh}_2\text{O}_3(\text{solid}) = 4/3\text{Rh} + \text{O}_2(\text{gas})$. The dependencies in Figure 2b take into account the values of equilibrium O_2 pressure measured upon dissociation of these oxides in the temperature range of 595–655, 717–797 and 770–930 K, respectively [22]. Regions of parameters above each curve correspond to the values at which the corresponding solid oxide is stable and under them—the neat metal. The dissociation heat values ($\Delta_{\text{diss}}H^0(T)$) of PtO_2 , PdO and Rh_2O_3 oxides, corresponding to the dependencies in Figure 2b, for the reactions listed above are equal to 222, 239 and 222 kJ/mol O_2 , respectively [22]. In the NH_3 oxidation reactor employed in this study, the pressure of the ammonia–air mixture is equal to 3.6 bar. At the NH_3 content of 10 vol.%, the O_2 pressure is 6.8×10^4 Pa. One can see in Figure 2b that the equilibrium P_{O_2} pressure grows from 10^{-5} to 6.8×10^4 Pa as the temperature is increased from 500 to 900 K for PtO_2 (1), from 600 to 1133 K for PdO (2), and from 650 to 1400 K for Rh_2O_3 (3). In addition, it follows from dependencies 1–3 in Figure 2b that at the O_2 pressure in the reactor (6.8×10^4 Pa) and the NH_3 oxidation temperature (ca. 1133 K) a stable state for Pt is the neat metal, while for

Rh—the solid oxide Rh_2O_3 . The dependence of equilibrium P_{O_2} for PdO (Figure 2b, curve 2) intersects the value of $P_{\text{O}_2} = 6.8 \times 10^4 \text{ Pa}$ at $T \sim 1133 \text{ K}$. It means that under the NH_3 oxidation conditions, at $T \leq 1133 \text{ K}$, the PdO solid oxide is stable, while at $T \geq 1133 \text{ K}$ —the metallic Pd. As a result, even a slight deviation of the reactor temperature from 1133 K may lead to the formation and/or decomposition of PdO oxide on Pd(poly).

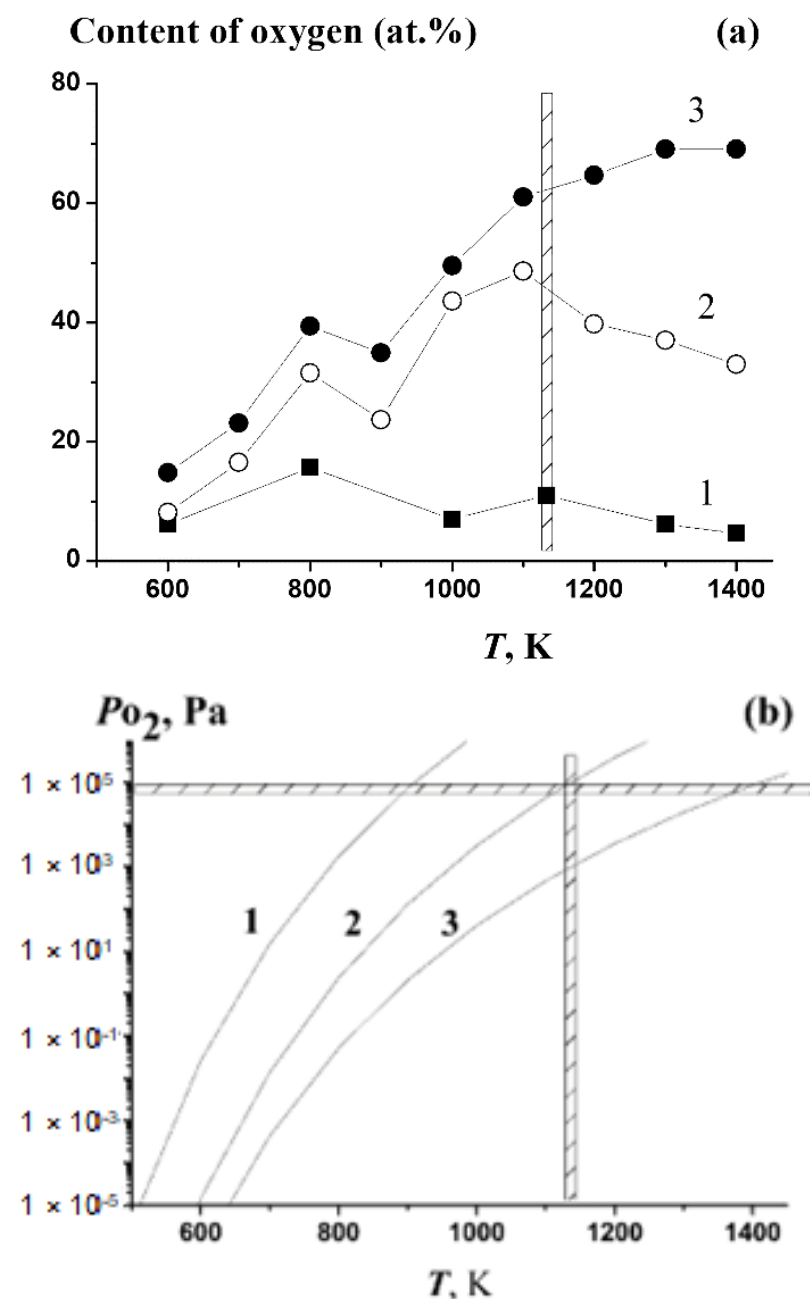


Figure 2. (a) Dependences of oxygen concentration on the temperature of treatment in O_2 for 3 h at $P_{\text{O}_2} = 2.1 \times 10^4 \text{ Pa}$ for Pt(poly) (1), and $P_{\text{O}_2} = 10^5 \text{ Pa}$ for Pd(poly) (2) and Rh(poly) (3) according to EDS data. (b) Temperature dependencies of equilibrium O_2 pressure during dissociation of $\text{PtO}_2(\text{solid})$ (1), $\text{PdO}(\text{solid})$ (2) and $\text{Rh}_2\text{O}_3(\text{solid})$ (3). The vertical dotted marker indicates the temperature of 1133 K, and the horizontal one— P_{O_2} equal to $6.8 \times 10^4 \text{ Pa}$.

Figure S1 (Supplementary Materials) displays the SEM images of the Pt(poly) surface after treatment in O_2 at 1100 K and $P_{\text{O}_2} = 1 \text{ bar}$ for 3 h. At low magnifications (Figure S1a,b), distinct grain boundaries separating grains with different brightness are detected on the

surface. At high magnifications (Figure S1c,d), a continuous layer of regular facets is observed on the grain surface. Parallel stepped crystal facets with a step height from 50 to 100–200 nm fill the entire surface of each grain. Flat layered facets ca. 10 nm in height are detected on the surface of such stepped facets (Figure S1d). The microfaceted surface of Pt(poly) was also observed in our earlier study after annealing in the O₂ atmosphere at 1300 K [21]. Figure 3 displays SEM images of the Pd(poly) (a–d) and Rh(poly) (e–h) surface after treatment of the samples in O₂ at 1100 K and $P_{O_2} = 1.0$ bar for 3 h. For Pd(poly), a continuous nonuniform layer containing fragments of different shapes and sizes that are separated with cracks 0.1–1.0 μm in width is detected at low magnifications (Figure 3a,b). The images in Figure 3a,b most likely demonstrate the partially decomposed surface oxide layer. Taking into account that the oxygen concentration in Pd(poly) after annealing in O₂ at 1100 K is equal to 48.6 at.% (Figure 2a), the oxide layer in Figure 3a–d can be attributed to PdO oxide. At high magnifications, crystal particles of PdO oxide with the size of 50–200 nm are detected in the oxide layer (Figure 3c). In the right and left parts of the image displayed in Figure 3c, one can see particles with such a size, which was estimated using the dimension mark in the image. In Figure 3c,d, a crack with a width of ca. 500 nm is observed in the oxide layer; it was used to estimate the thickness of the oxide layer at 100–200 nm. In addition, a crystal Pd facet with a height of ca. 100 nm is detected in this crack.

For Rh(poly), a continuous dark layer is detected at low magnifications; a vertical strip ca. 10 μm in width consisting of bright particles is seen at the center of this layer (Figure 3e). Images in Figure 3f,g show spherical particles with a size of 100–200 nm. One can see in Figure 3h that these particles reside in a continuous layer comprising 25–50 nm particles. Taking into account that the oxygen concentration in Rh(poly) after annealing in O₂ at 1100 K is equal to 61.1 at.% (Figure 2a), the surface layer in Figure 3e–h can be attributed to Rh₂O₃ oxide. For Rh, Pt and Pd, the 1100 K value is close to the Tamman temperature ($T/T_{\text{melt}} \sim 0.5$) for these metals because the T/T_{melt} value for them is 0.49, 0.54 and 0.6, thus indicating high mobility of atoms of these metals. As a result, recrystallization and oxidation processes, forming the oxide particles and crystal facets on the grain surface, proceed very intensely. According to Figure 2a, at 1100 K in the O₂ atmosphere, the oxygen concentration on Pt(poly) is ca. 10.0 at.%, on Pd(poly)—48.6 at.%, and on Rh(poly)—61.1 at.%. On Pt(poly), O atoms are accumulated on such defects as grain boundaries and dislocations; the dissolution of oxygen in the metal lattice is not observed [21]. On Pd(poly) and Rh(poly), O atoms both penetrate the defects and intercalate in the lattice of metals. These processes lead to the formation of particles and/or crystals of PdO and Rh₂O₃ oxides on the Pd and Rh surfaces. This is demonstrated by SEM images of the surface of samples after annealing in O₂ at 1100 K. For Pt(poly), the observed surface is typical of the recrystallized polycrystalline metallic sample (Figure S1). For Pd(poly), one can see a cracked and partially decomposed 100–200 nm thick oxide layer of PdO particles and/or crystals with a size of 50–200 nm (Figure 3a–d). For Rh(poly), a continuous oxide layer of Rh₂O₃ oxide particles with the size of 25–50 nm is observed, which contains large particles and/or oxide crystals with the size of 100–200 nm (Figure 3e–h). These results are consistent with the data on equilibrium O₂ pressure for dissociating PtO₂, PdO and Rh₂O₃ oxides (Figure 2b). For $P_{O_2} = 1$ bar and $T = 1100$ K used in the study, stable for Pt is the metallic state (Figure 2b, curve 1). For Pd, the dependence of equilibrium P_{O_2} for PdO (Figure 2b, curve 2) intersects the value of $P_{O_2} = 1$ bar at $T \sim 1100$ K, which indicates that the formation and decomposition of PdO solid oxide can occur under the indicated conditions. For Rh, under such conditions, the solid oxide Rh₂O₃ is stable (Figure 2b, curve 3).

The data obtained on the oxidation of Pt(poly), Pd(poly) and Rh(poly) were used to elucidate the effect exerted by the oxidation of metal on its etching initiated by NH₃ oxidation with air oxygen. According to SEM and EDS data, after NH₃ oxidation with air oxygen at $T = 1133$ K and the reactor pressure of 3.6 bar for 1, 5 and 10 h, etched structures of different chemical compositions appear on the surface of Pt(poly), Pd(poly) and Rh(poly). The structures detected after NH₃ oxidation strongly differs from those observed after annealing in O₂.

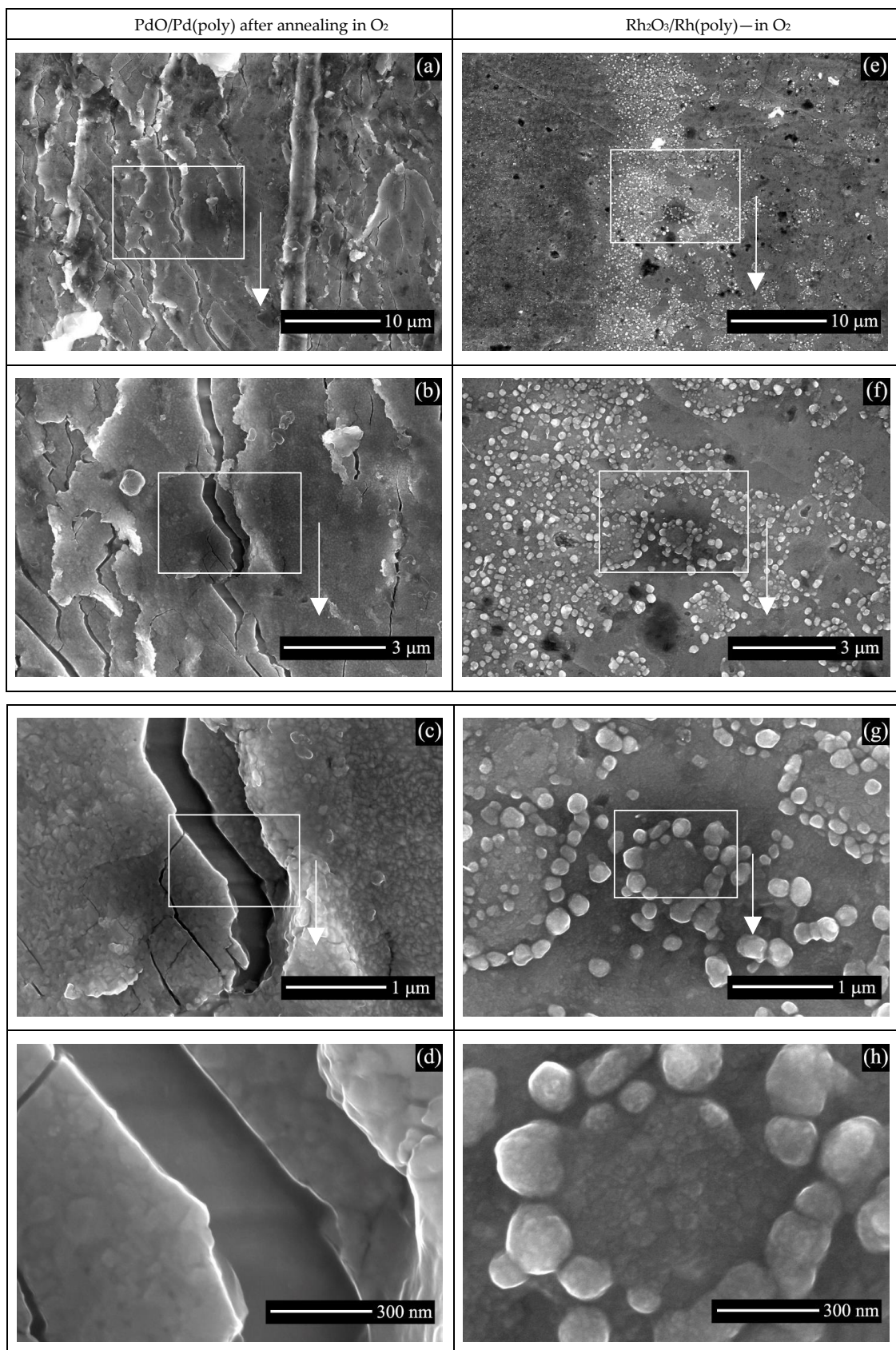


Figure 3. SEM image of the surface of samples Pd(poly) (a–d) and Rh(poly) (e–h) after annealing in O₂ at $P_{O_2} = 1$ bar and 1100 K for 3 h. Images were obtained in SE mode at $E_0 = 20$ keV; rectangles indicate the regions represented by images with a higher magnification.

2.3. Morphology and Chemical Composition of Pt(poly), Pd(poly) and Rh(poly) after NH₃ Oxidation with Air at 1133 K for 1, 5 and 10 Hours

Pt(poly) after NH₃ oxidation. Figure 4 displays SEM images of the Pt(poly) surface after NH₃ oxidation with air oxygen at $T = 1133$ K for 1 (a–d) and 5 (e–h) hours. Images obtained at low magnifications (Figure 4a,b,e,f) show considerable changes in the surface morphology compared to the new Pt(poly) sample (Figure 1a) and the sample after annealing in O₂ (Figure S1). After NH₃ oxidation for 1 h, a granular structure with ca. 50–100 μm bright and dark grains separated by distinct grain boundaries is observed on the Pt(poly) surface (Figure 4a,b). The surface of the bright grains contains regular parallel grooves (facets), which are similarly separated. In contrast, the surface of dark grains contains irregular facets and hollows, which have smaller sizes and lower concentrations than the facets on bright grains (Figure 4c,d). Images obtained at high magnifications (Figure 4c,d) demonstrate significant differences in the etching structures on adjacent grains. In the left part of images in Figure 4c,d, each grain contains facets with a close orientation, which differs from the orientation of the facets on adjacent grains. Crystal facets in Figure 4c,d have a step height of up to 0.5–1.0 μm . Differences in the etching structures of adjacent grains may be related to the different surface orientations of these grains, which can substantially affect the faceting during NH₃ oxidation.

After NH₃ oxidation for 5 h, a granular structure with a grain size of 50–100 μm is also detected on the Pt(poly) surface (Figure 4e,f). The grain surface has close brightness; each grain contains etched structures represented by extended, parallel and similarly separated facets. Images obtained at high magnifications show a distinct grain boundary and large crystal facets with a step height of up to 1–2 μm (Figure 4g,h). This sample was used in NH₃ oxidation for an additional 5 h. After NH₃ oxidation for 10 h, distinct grain boundaries, which separate grains with parallel facets having a step height of up to 1–2 μm , are seen on the sample surface. The revealed structure is close to that obtained after the oxidation for 5 h (Figure 4e–h).

Thus, after NH₃ oxidation on Pt(poly) at 1133 K for 1, 5 and 10 h, the microgranular structure of metallic platinum with a grain size of 50–100 μm is detected on the surface. The grain surface predominantly contains regular, similarly separated crystal facets. In all cases, particles and/or crystals of such platinum oxides as PtO₂ were not observed. This is consistent with the temperature dependence of equilibrium O₂ pressure above PtO₂(solid), which testifies to the stable metallic state of Pt under the conditions of NH₃ oxidation used in this study (Figure 2b). In addition, a comparison of images of the Pt(poly) surface after annealing in O₂ (Figure S1) and after NH₃ oxidation (Figure 4) at a temperature of ca. 1100 K shows their close microstructures. In both cases, the microgranular structure of metallic platinum with the faceted grain surface was observed; however, after annealing in O₂, the height of facets is 100–200 nm, while after NH₃ oxidation, facets with a size up to 1–2 μm are detected. This indicates that the etching of the Pt(poly) surface is more intense during the catalytic oxidation of NH₃ as compared to annealing in O₂. In [11], after NH₃ oxidation for 386 h, both the terraces 5–10 μm in width with ca. 1 μm high facets, and crystal “cauliflowers” with the size of 5–20 μm were found on the surface of platinum wire.

The concentration of elements on Pt(poly) after NH₃ oxidation was estimated from the EDS data obtained by the accumulation of EDS spectra for 150 s in three square regions of the surface with the size of 5×5 μm , which are located on different grains. The EDS spectra were recorded on the surface regions similar to those displayed in Figure 4c,g. Pt, C, O and N were detected on all surface regions for all Pt(poly) samples. In addition, it should be noted that on some regions Fe, Si, Al and Mg impurities were detected in a low concentration, ≤ 0.1 –0.5 at.%. Concentrations of these elements strongly differ on different regions and may be associated with the impurities that were present in the initial material or transferred to the catalyst from the gas flow and reactor during the oxidation of NH₃. Note also that concentrations of these elements were measured with a relatively high statistical error at the detection limit of this method. As a result, the indicated impurities may have low concentrations or be completely absent. Taking into account the indicated

data, Fe, Si, Al and Mg elements were excluded from the list of detected elements, and only the main Pt, C, O and N elements were considered.

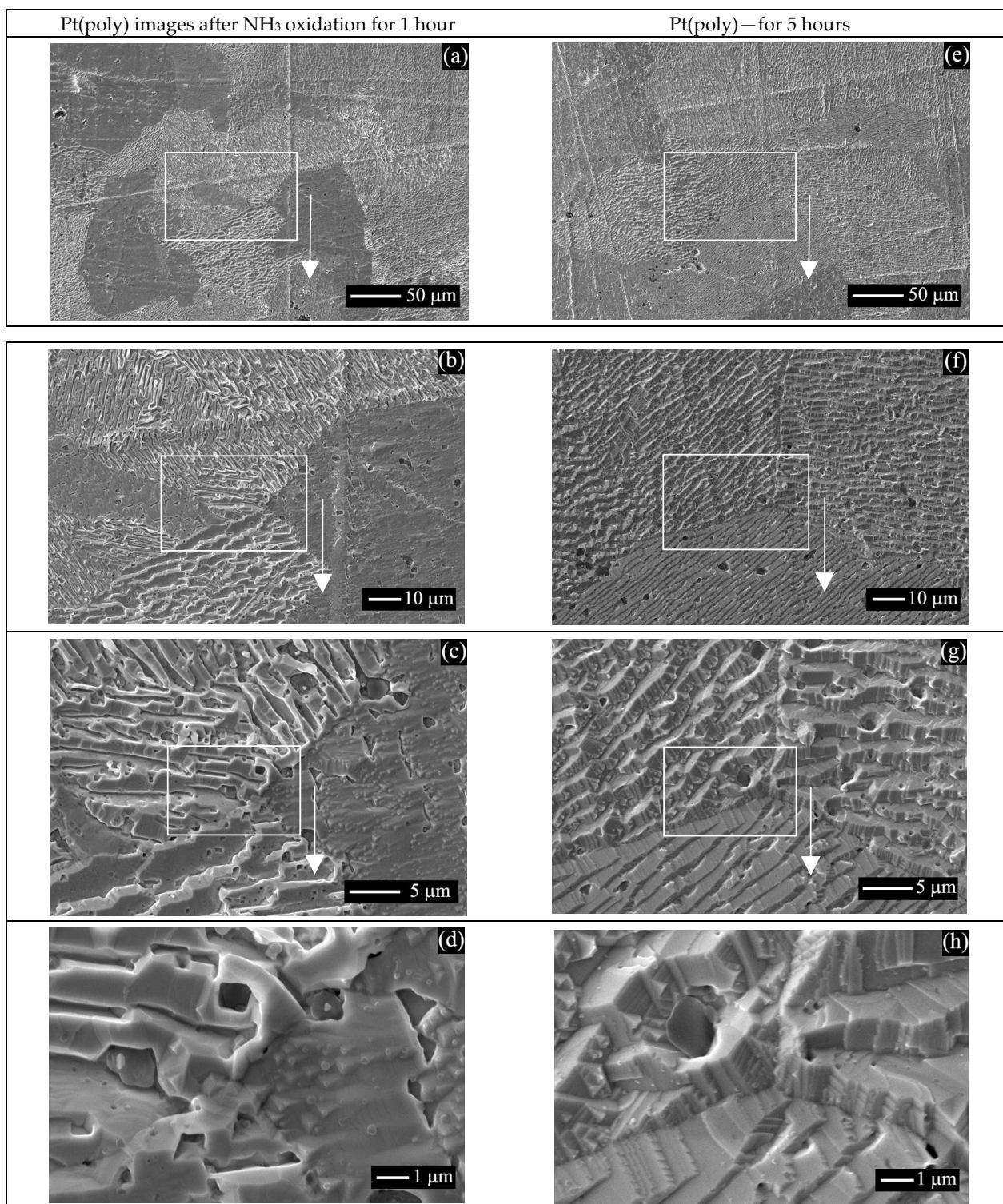


Figure 4. SEM images of the Pt(poly) surface after NH_3 oxidation with air oxygen at $T = 1133$ K for 1 (a–d) and 5 (e–h) hours. Images were obtained in SE mode at $E_0 = 20$ keV; rectangles indicate the regions represented by images with a higher magnification.

Figure 5 displays data on the chemical composition of the Pt(poly) (a–c) and Rh(poly) (d–f) after NH_3 oxidation at 1133 K for 1 (a,d), 5 (b,e) and 10 (c,f) hours according to EDS

data. The concentrations of Pt, C, O and N in the three squares differed insignificantly from each other, so they were used to calculate the average concentrations. Figure 5 indicates the obtained averaged concentrations of these elements after NH₃ oxidation for 1 (a), 5 (b) and 10 (c) hours. After NH₃ oxidation for 1 h, the concentrations of Pt, C, O and N were equal to 60.7, 29.3, 5.7 and 4.3 at.%, respectively (Figure 5a). It should be noted that the obtained oxygen concentration (5.7 at.%) was close to that obtained after annealing of Pt(poly) in O₂ at 1133 K (ca. 10.0 at.%, as shown in Figure 2a). It should also be noted that C and O were detected on some regions of the new Pt(poly) sample in the concentration of ca. 28.2 and 0.7 at.%, respectively. The detected carbon may include C atoms as the absorbed C_{ab} atoms on such defects as dislocations and grain boundaries in subsurface layers of the sample. Most likely, O and N atoms detected by EDS include predominantly the O_{ab} and N_{ab} atoms that were absorbed on defects in subsurface platinum layers. As the NH₃ oxidation time is extended from 1 to 5 and 10 h, a gradual decrease in the concentration of C (29.3, 26.6, 21.0 at.%) and its growth for O (5.7, 10.1, 10.9 at.%) are observed. The N concentration remains virtually constant, equal to 4.3, 6.4 and 5.2 at.%. Changes in the concentration of detected C and O with the extension of the NH₃ oxidation time testify to a gradual removal of C_{ab} from the subsurface region and accumulation of O_{ab} atoms in this region.

Rh(poly) after NH₃ oxidation. Figure 6 displays images of the Rh(poly) surface after NH₃ oxidation with air oxygen at $T = 1133$ K for 1 (a–d) and 5 (e–h) hours. Images obtained at low magnifications (Figure 6a,e) demonstrate considerable changes in the surface morphology after NH₃ oxidation compared to the new Rh(poly) (Figure 1e), and the sample annealed in the O₂ atmosphere, as shown in Figure 3e–h. After NH₃ oxidation for 1 h, bright agglomerates, ca. 1 μm in diameter and extended agglomerates, ca. 1–2 μm in width and up to 30 μm in length, are observed on the Rh(poly) surface, as shown in Figure 6a,b. Images obtained at high magnifications (Figure 6c,d) show a continuous dark layer comprising particles with the size of ca. 0.5–1.0 μm, on which bright agglomerates with the fibrous structure reside. Fibers detected at high magnifications have a diameter of 25–50 nm. The revealed etching structure on the Rh(poly) surface, which was formed during the oxidation of NH₃ for 1 h, is determined by a strong effect exerted by the oxidation of rhodium on its etching under the indicated conditions. According to the dependence of equilibrium O₂ pressure above Rh₂O₃ oxide, at the O₂ pressure used in the study and $T \leq 1400$ K, the Rh₂O₃ oxide is stable, as shown in Figure 2b, curve 3. In addition, after the oxidation of Rh(poly) in O₂ at 1100 K, a continuous Rh₂O₃ oxide layer consisting of particles with the size of 25–50 nm was observed. Spherical crystal particles with the size of 100–200 nm were detected in this layer, as shown in Figure 3e–h. These data allow a conclusion that the NH₃ oxidation on Rh(poly) at 1133 K for 1 h leads to the formation of a continuous surface oxide layer consisting of particles and/or crystals of Rh₂O₃ oxide with the size of 0.5–1.0 μm, as shown in Figure 6d. During the oxidation of NH₃ molecules, metal-oxide nanofibers and nanocrystals with the size of 25–50 nm emerge on the oxide layer. They gradually form metal-oxide fibrous agglomerates with a size of ca. 1 μm and agglomerates with a length of up to 30 μm, as shown in Figure 6a–d. It should be noted that in [12], after NH₃ oxidation for 23 h, “wool”-like and whisker deposits of Rh₂O₃ and “cauliflowers” with the size of 3–80 μm were detected on the surface of rhodium wire.

After NH₃ oxidation on Rh(poly) for 5 h, a layer of bright particles with a size below 1 μm is observed on the sample surface, as shown in Figure 6e,f. Images obtained at high magnification show a continuous layer of pyramidal crystals oriented from the surface, as shown in Figure 6g,h. In the initial step of NH₃ oxidation ($t = 1$ h), a continuous Rh₂O₃ oxide layer is formed on the Rh(poly) surface. During the further oxidation of NH₃ ($t = 5$ h), pyramidal crystals emerge on the surface of this oxide and gradually fill the entire surface. The crystals have a length of 1–2 μm, and their sizes are equal to 0.3–0.5 μm at the pyramid’s base and 0.05–0.1 μm at its vertex, as shown in Figure 6h. After NH₃ oxidation on Rh(poly) for 10 h, a continuous etched layer of pyramidal crystals appears on the surface; the crystals are 1–2 μm in length, and their sizes are equal to 0.4–0.5 μm at the base of the pyramid and 0.1–0.2 μm at their vertices.

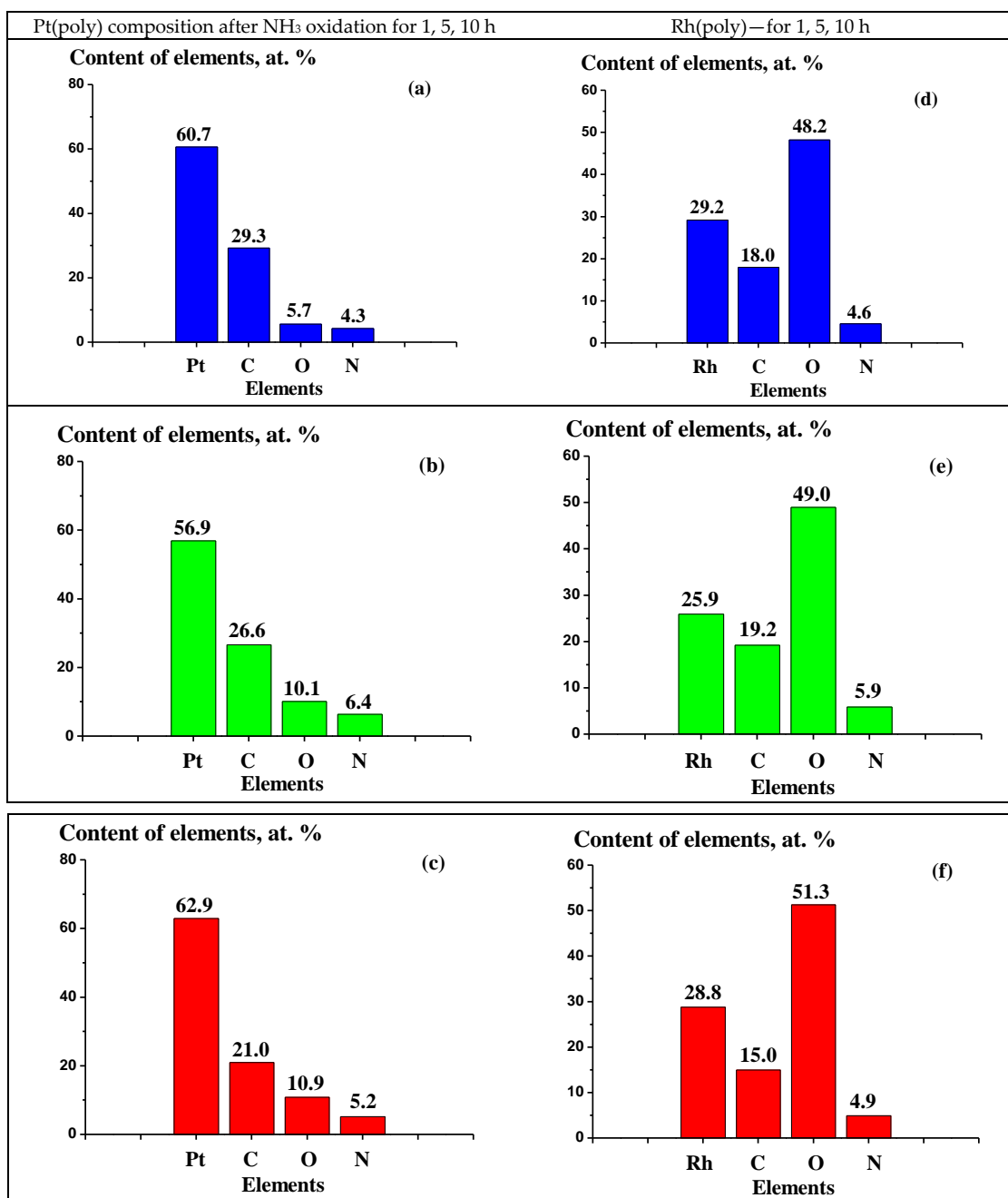


Figure 5. Concentrations of Pt, Rh and C, O, N on Pt(poly) (a–c) and Rh(poly) (d–f) after NH_3 oxidation at 1133 K for 1 (a,d), 5 (b,e) and 10 (c,f) hours according to EDS data obtained at a probe electron energy $E_0 = 20$ keV.

Figure 5d–f illustrate data on the chemical composition of the Rh(poly) subsurface layer after NH_3 oxidation for 1 (d), 5 (e) and 10 (f) hours. The concentrations of the main elements and impurities were estimated similarly as for Pt(poly) (see above) from the EDS data obtained by the accumulation of EDS spectra on the surface regions with the size of $15 \times 15 \mu\text{m}$. Rh, C, O and N were detected on all surface regions for all Rh(poly) samples. Figure 5d–f indicates the averaged concentrations of these elements. After NH_3 oxidation for 1 h, the concentrations of Rh, C, O and N equal 29.2, 18.0, 48.2 and 4.6 at.%, respectively, as shown in Figure 5d. It should be noted that the measured O concentration (48.2 at.%) is close to the value obtained after the oxidation of Rh(poly) in O_2 at 1100 K (61.1 at.%, as shown in Figure 2a) but considerably exceeds the O concentration on the new sample (ca. 7.3 at.%). The obtained oxygen concentration testifies to the formation of Rh_2O_3 oxide

during the oxidation of NH_3 . The detected carbon may include C atoms residing on the surface and in subsurface layers of the sample. The detected oxygen corresponds mostly to O^{2-} ions of Rh_2O_3 oxide and nitrogen—to N_{ab} atoms absorbed on defects in the subsurface layer of the catalyst. An extension of the NH_3 oxidation time on Rh(poly) (1, 5 and 10 h) produces slight changes in the concentrations of elements: an increase for O (48.2, 49.0 and 51.3 at.%), a decrease for C (18.0, 19.2 and 15.0 at.%), and minor deviations for N (4.6, 5.9 and 4.9 at.%) and Rh (29.2, 25.9 and 28.8 at.%), as shown in Figure 5d–f. The concentrations of elements on Rh(poly) samples measured after NH_3 oxidation for 1, 5 and 10 h indicate that the oxidation of NH_3 proceeds on the surface of the Rh_2O_3 oxide layer for the entire period.

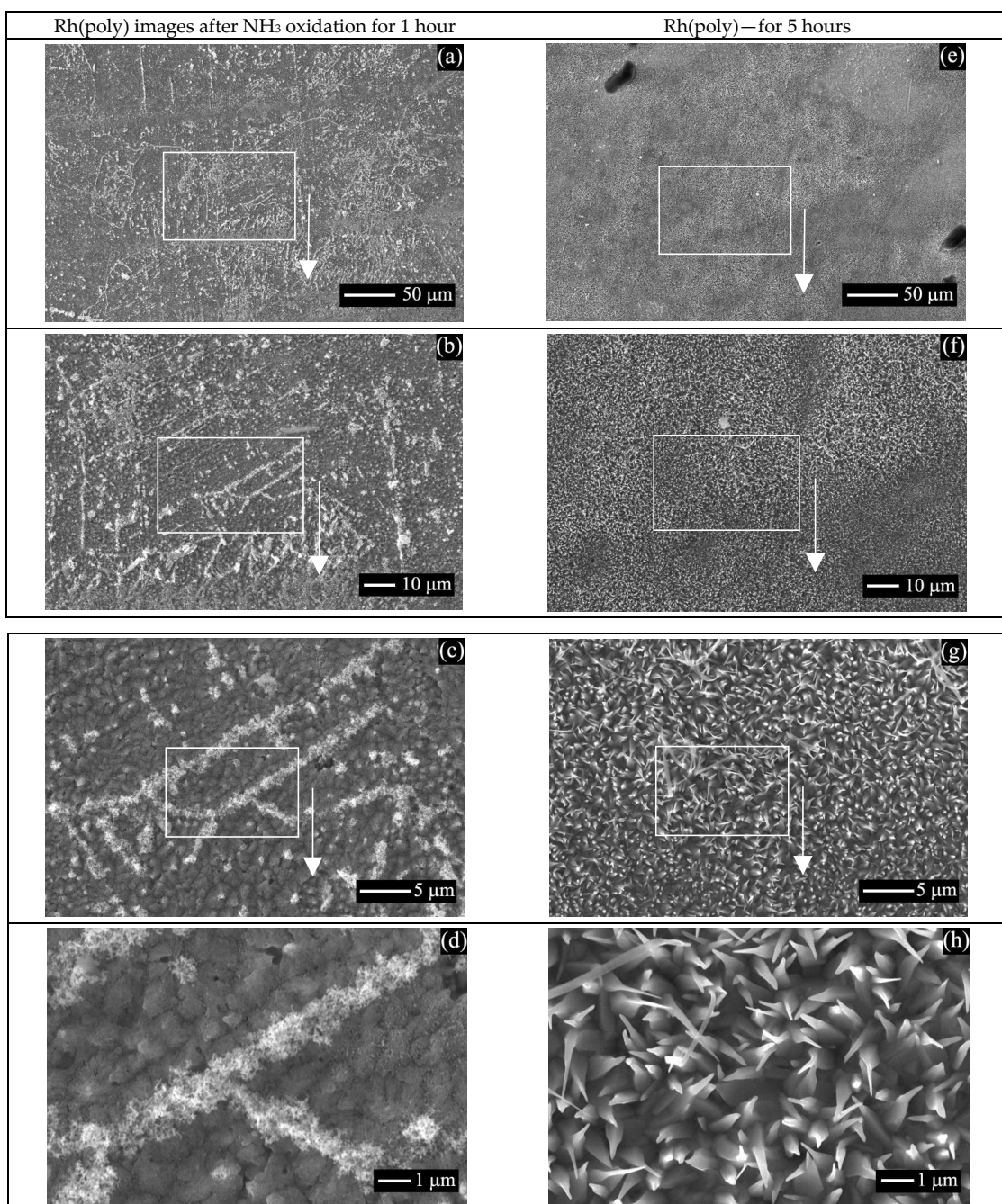


Figure 6. SEM images of the Rh(poly) surface after NH_3 oxidation with air oxygen at $T = 1133$ K for 1 (a–d) and 5 (e–h) hours. Images were obtained in SE mode at $E_0 = 25$ keV; rectangles indicate the regions represented by images with a higher magnification.

Pd(poly) after NH_3 oxidation. Figure 7 displays SEM images of the Pd(poly) surface after NH_3 oxidation with air oxygen at $T = 1133$ K for 1 (a–d) and 5 (e–h) hours. Images obtained at low magnifications (Figure 7a,e) show essential changes in the surface morphology compared to the new Pd(poly) (Figure 1c) and the sample annealed in O_2 (Figure 3a–d). After NH_3 oxidation for 1 h, we observed on the Pd(poly) surface a continuous layer of agglomerates with a diameter of 1–5 μm and extended agglomerates having a width of ca. 1–5 μm and a length from 5 to 30 μm , as shown in Figure 7a,b. SEM images obtained at high magnifications (Figure 7c,d) demonstrate these agglomerates' loose, fibrous surface structure. Fibers detected at high magnifications have a thickness in the range of 25–50 nm. The etched structure revealed on the Pd(poly) surface is caused by a considerable effect of Pd oxidation on its etching under the conditions of NH_3 oxidation. First of all, it should be noted that during the oxidation of NH_3 for 1 h the catalyst temperature may strongly deviate from the maintained value of ca. 1133 K. Taking into account a short period of NH_3 oxidation in this experiment ($t = 1$ h), low values of the catalyst temperature (<1133 K) can be expected. Thus, after feeding the reaction mixture into the reactor, a ca. 1133 K temperature on the gauzes is reached approximately for 5 min during the exothermic oxidation of NH_3 . It seems that the Pd(poly) sample is heated to this temperature much more slowly because the temperature mode is generally maintained by the exothermic oxidation of NH_3 on catalytic gauzes. After 1 h of NH_3 oxidation, feeding of NH_3 and, accordingly, heating of the catalyst and reactor was stopped, and the catalyst was gradually cooled to ca. 300 K for ca. 30 min. Taking into account the oxidation time of NH_3 as well as the estimated time of catalyst heating and cooling, one can suppose that the temperature of Pd(poly) sample could be lower than 1133 K for a substantial part of this period. According to Figure 2b, curve 2, at $T < 1133$ K and O_2 pressure used in the study, the PdO oxide is stable. In addition, after annealing of Pd(poly) in O_2 at 1100 K, a 100–200 nm thick nonuniform surface layer consisting of PdO particles with the size of 50–200 nm was found (Figure 3a–d). The reaction of NH_3 molecules with the oxygen of the oxide layer leads to the emergence of metal-oxide nanofibers and nanocrystals with the size of 25–50 nm, which gradually form metal-oxide fibrous agglomerates ca. 1–5 μm in size and agglomerates with a length up to 5–30 μm (Figure 7a–d). It should be noted that in [13] NH_3 oxidation for 54 h resulted in the formation of terraces, facets, “cauliflowers”, “wool”-like deposits of PdO, and a continuous PdO oxide layer with a thickness of ca. 4 μm on the surface of palladium wire.

After NH_3 oxidation for 5 h, a continuous etched layer comprising crystals and porous crystal “cauliflowers” with different shapes and sizes of 10–30 μm is observed on the Pd(poly) surface, as shown in Figure 7e,f. Such “cauliflowers” contain pores with a diameter 1–2 μm and are separated by extended voids 1–10 μm in width, as shown in Figure 7g,h. After NH_3 oxidation for 54 h, palladium “cauliflowers” with the size of 4–55 μm were detected on the surface of palladium wire [13]. In addition, images of crystal “cauliflowers” in Figure 7e–h are close to the earlier obtained images of metallic “cauliflowers” on Pt–Pd–Rh–Ru gauzes after NH_3 oxidation at 1133 K for 50 h [16,17]. Taking into account this information, the etched layer observed on the Pd(poly) surface (Figure 7e–h) indicates the formation of palladium “cauliflowers” during the oxidation of NH_3 at 1133 K for 5 h. Heating of the catalyst after feeding the NH_3 flow and cooling of the catalyst after turning off the flow were performed for ca. 5 and 30 min, respectively. This constitutes an insignificant part of this experiment's entire period of NH_3 oxidation ($t = 5$ h). As a result, upon NH_3 oxidation for 5 h, the Pd(poly) sample is kept mostly at $T \sim 1133$ K. In addition, the catalyst temperature during NH_3 oxidation may deviate to both sides from the maintained value (ca. 1133 K). Under the indicated conditions, the formation-decomposition of PdO oxide can proceed on Pd(poly) because, at the P_{O_2} value used in this study and $T < 1133$ K, the PdO oxide is stable, whereas at $T > 1133$ K—the metallic palladium (Figure 2b, curve 2). In addition, the reaction of NH_3 with the oxygen of PdO oxide will lead to the decomposition of the oxide particles. These processes will result in a gradual formation of palladium “cauliflowers”. As a result, after 5 h of NH_3 oxidation at $T \sim 1133$ K, a continuous etched layer of “cauliflowers” is observed on Pd(poly)

(Figure 7e–h). It should be noted that after 5 h of NH_3 oxidation, deep cracks destroying the sample appeared on Pd(poly); these cracks made it impossible to mount the sample in the reactor and perform NH_3 oxidation for another 5 h. In [13], after NH_3 oxidation for 54 h, the destruction of palladium wire was also observed.

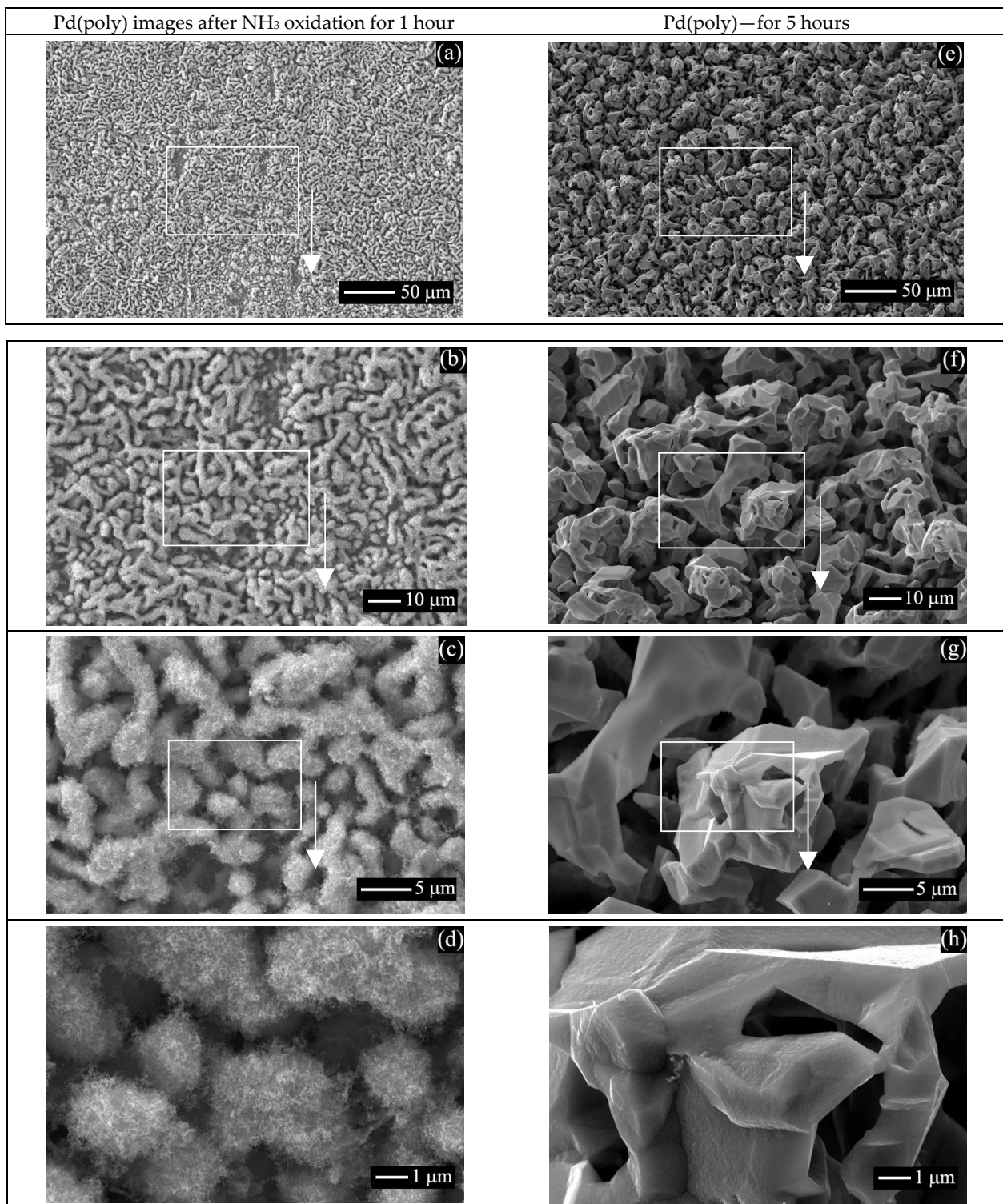


Figure 7. SEM images of the Pd(poly) surface after NH_3 oxidation with air oxygen at $T = 1133$ K for 1 (a–d) and 5 (e–h) hours. Images were obtained in SE mode at $E_0 = 25$ keV; rectangles indicate the regions represented by images with a higher magnification.

Figure S2 (Supplementary Material) displays data on the chemical composition of the Pd(poly) subsurface layer after NH₃ oxidation for 1 (a) and 5 (b) hours. The concentrations of the main elements and impurities were estimated in a similar manner as for Pt(poly) (see above) from the EDS data obtained by the accumulation of EDS spectra on the surface regions with the size of 35 × 35 μm after NH₃ oxidation for 1 h (Figure 7a) and 5 × 5 μm—for 5 h (Figure 7f). Pd, C, O and N were detected on all surface regions for all Pd(poly) samples.

In Figure S2, one can see the averaged concentrations of these elements. After NH₃ oxidation for 1 h, the concentrations of Pd, C, O and N were equal to 51.7, 4.1, 39.2 and 5.0 at.%, respectively, as shown in Figure S2a. Note that the observed O concentration (39.2 at.%) is close to the value obtained after annealing of Pd(poly) in O₂ at 1100 K (48.6 at.%, Figure 2a) but considerably exceeds the O concentration (ca. 0.0 at.%) measured on the new sample. The detected carbon may be associated with C impurities in subsurface Pd layers. The detected nitrogen may correspond mostly to the N_{ab} atoms absorbed on defects in the subsurface layers of the catalyst. An extension of the NH₃ oxidation time from 1 to 5 h is accompanied by a significant decrease in the concentration of O (from 39.2 to 2.0 at.%) and C (from 4.1 to 2.3 at.%) and noticeable growth of the N content (from 5.0 to 11.3 at.%), as shown in Figure S2a,b. Changes in the surface morphology and O concentration on Pd(poly) that occur with extension of the NH₃ oxidation time indicate that the oxidation of NH₃ proceeds mostly on PdO oxide at the very onset of the process (at $t = 1$ h) and later on palladium “cauliflowers” (at $t = 5$ h).

2.4. Structural Characteristics of New Pt(poly), Pd(poly) and Rh(poly) and Those after NH₃ Oxidation with Air at 1133 K for 5 and 10 Hours

The phase composition of new Pt, Pd and Rh foils, and those used in NH₃ oxidation was studied by XRD. Figure 8 displays the diffraction patterns obtained in the range of diffraction angles (2θ) from 30 to 115° for new samples (a–c) and also for those after NH₃ oxidation at 1133 K during 10 (d,f) and 5 h (e) for the Pt(poly) (a,d), Pd(poly) (b,e) and Rh(poly) (c,f). The indicated diffraction patterns contain the diffraction peaks for these metals, which are denoted by indices (*hkl*).

For Pt used in NH₃ oxidation (Figure 8d), one can see considerable changes in the intensity of diffraction peaks (111), (220) and (311) in comparison with the peaks for the initial Pt (Figure 8a). This testifies to textural changes of the Pt(poly) surface layer during the etching process. For Pd (Figure 8b,e) and Rh (Figure 8c,f), changes in these peaks are also detected, but they are not so pronounced in comparison with Pt. The recorded diffraction patterns were used to calculate the face-centered cubic (fcc) cell parameter of the lattice of metals (*a*). The calculation was performed in the same manner as for Pt alloy gauzes employed in the oxidation of NH₃ at 1133 K [17] and for Pt(poly) after annealing in O₂ at 600–1400 K [21]. For new samples and those used in NH₃ oxidation, the calculation gives the following values of *a*: for Pt—3.920, 3.922 Å, for Pd—3.888, 3.889 Å, and for Rh—3.800, 3.800 Å. The obtained *a* values for new metals and those after NH₃ oxidation are close to each other. In addition, these *a* values are close to the values for neat metals indicated in the X-ray diffraction database (PDF): for Pt—3.923 Å (PDF # 04-0802), for Pd—3.888 Å (PDF # 46-1043), and for Rh—3.803 Å (PDF # 05-0685). The obtained *a* values testify to the stable state of these metals to a depth up to 10 μm during NH₃ oxidation since the depth of XRD analysis is ca. 10 μm [21]. In addition, it should be noted that additional peaks indicating other phases, particularly the carbide and oxide ones, were not detected on Pt and Pd. Whereas for Rh used in the oxidation of NH₃, intense peaks are observed (Figure 8f), which coincide with those indicated in the PDF database for the β-Rh₂O₃ oxide (PDF # 43-0009). The obtained structural characteristics testify to the stable metallic state of Pt, Pd and Rh and the formation of the Rh₂O₃ surface oxide layer on Rh(poly) during NH₃ oxidation, which is generally consistent with the SEM and EDS data on the state of Pt, Pd and Rh during the oxidation of NH₃ for 5 and 10 h (see above).

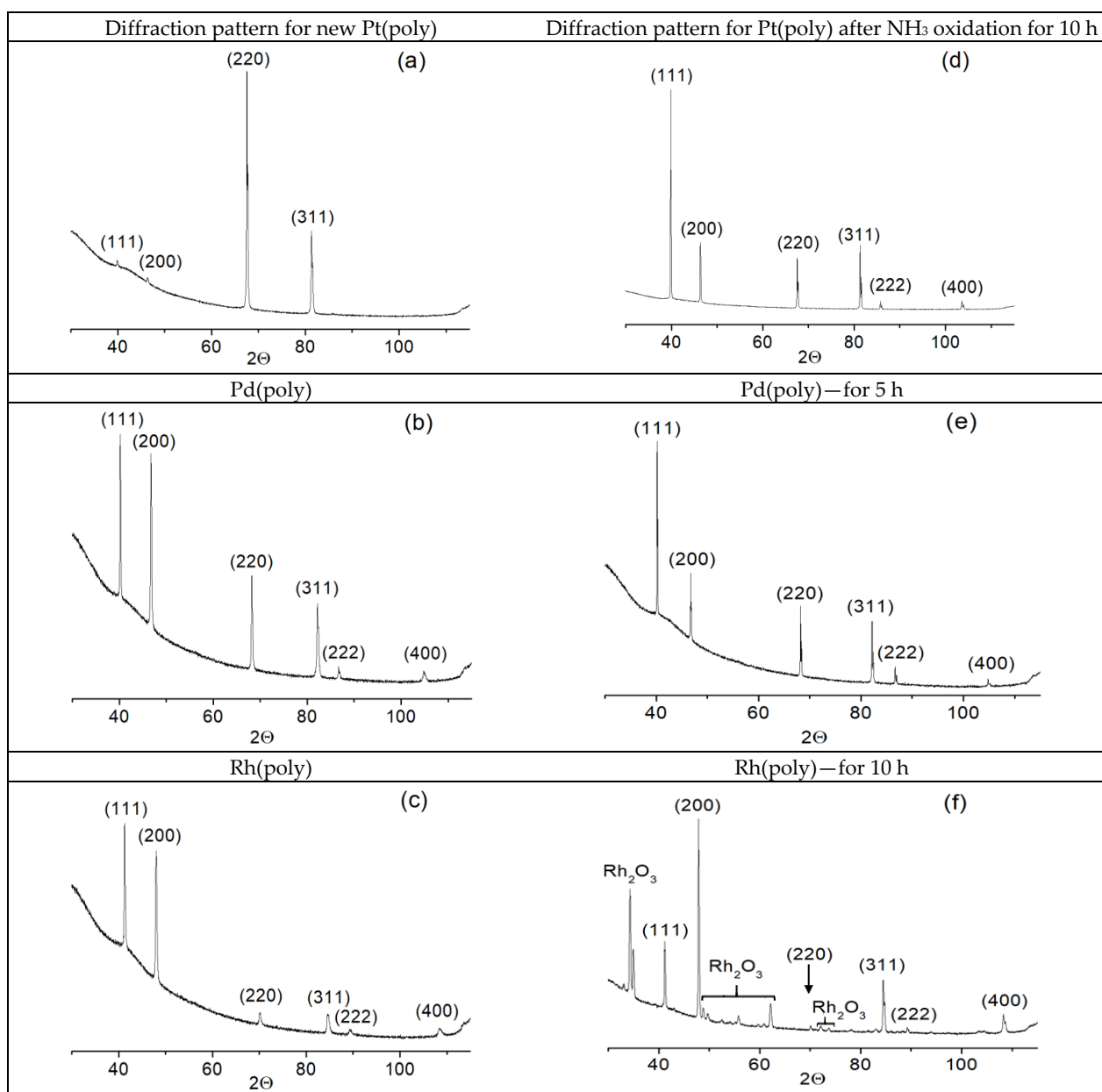


Figure 8. X-ray diffraction patterns for the new foils (a–c) as well as after NH_3 oxidation with air at 1133 K (d–f) during 5 (e) and 10 h (d,f) for the Pt(poly) (a,d), Pd(poly) (b,e) and Rh(poly) (c,f).

3. Discussion

The application of Pt–Rh and Pt–Pd–Rh gauzes considerably enhances the performance of NH_3 oxidation as compared to neat Pt [5,6]. Thus, the use of Pt/5–10 wt.% Rh alloys increases NO yield at 1073–1173 K by 3.0–5.0% compared with neat Pt (~94%) [6]. The addition of up to 1 wt.% Ru or ca. 7 wt.% Rh or Pd to Pt increases approximately twofold the ultimate strength of the alloy compared to neat platinum [5]. The application of such alloys considerably reduces catalyst losses and increases the mechanical strength and operation time of the gauzes [5,6]. In addition, Pd–Au and Pd–Ni alloys are used for the production of catchment gauzes [23–25]. They are applied to capture $\text{PtO}_2(\text{gas})$, which appreciably decreases Pt losses during industrial NH_3 oxidation on Pt alloys gauzes. The high-temperature oxidation of NH_3 with air oxygen to NO oxide on platinum alloy gauzes is accompanied by a deep structural rearrangement of the surface of metal catalysts (catalytic etching) [3–5,7]. The observed catalytic etching is attributed to the mass transfer of metals caused by the increased mobility of surface atoms and the emergence of super-

equilibrium concentration of the adsorbed metal atoms and their diffusion over the surface during NH_3 oxidation (see, for example, [11,15,16]). In [11–13], the mass transfer of metals and surface rearrangement in the process of NH_3 oxidation with oxygen on Pt, Rh, Pd, Ag, Ir and Pt–Rh, Pt–Ir, Pd–Ni alloys are associated with the transport of volatile oxides ($\text{PtO}_2(\text{gas})$, $\text{RhO}_2(\text{gas})$ and others) and metals ($\text{Pd}(\text{gas})$, $\text{Ag}(\text{gas})$), which are formed on the hot surface regions, to the cold regions of the catalyst surface by the CVT mechanism. The transfer occurs due to the formation of “hotspots” in the region of defects on the catalyst surface in the course of a strongly exothermic reaction of NH_3 oxidation with oxygen. It should be noted that catalytic etching is observed for many catalytic systems [26–29], for example, in the oxidation of C_3H_8 on Ni [26], C_1 – C_4 alkanes on Ni and Pd [27], and CO on Co [28]. In [29], general problems of thermal etching in an inert atmosphere and catalytic etching during the oxidation of H_2 , CO, CH_4 , NH_3 and synthesis of HCN are discussed for a series of metals Pt, Pd, Ag, Cu, Fe, Ni, etc.

In both cases, changes in the morphology are revealed; however, at catalytic etching, the morphology of a metal changes much more rapidly and strongly than in the case of thermal etching. In addition, noteworthy is a strong dependence of catalytic etching on the catalyst composition and structure, its temperature and the composition of the reaction medium. A decrease in the catalyst surface energy due to the faceting of the surface structures is discussed as a driving force of etching. Surface and bulk diffusion, as well as evaporation-condensation, are considered to be the mass transfer processes leading to the rearrangement of the catalyst surface [29].

3.1. Oxidation of PGMs (Pt, Pd and Rh)

Despite the high chemical and etching resistance and the high-temperature stability of PGMs [1], they are subjected to oxidation and etching in the reaction media, particularly under catalytic oxidation reactions [26]. The catalytic etching and losses of metals, which are observed during the high-temperature oxidation of NH_3 to NO on platinum alloy gauzes, may also be related to the oxidation of metals, including the formation of volatile and solid oxides of metals. Pt, Pd and Rh, which are employed to obtain alloys for the production of Pt alloy gauzes, are also prone to oxidation and etching in the oxidizing medium [9,10]. In [9,10], O_2 , air, H_2O , vacuum, N_2O , NO, etc., were shown to exert different actions on the transport of metals and surface morphology of Pt, Rh and Pt–Rh alloys at a temperature of 973–1473 K. For Pt, Rh, Pt/5%Rh, Pt/30%Rh and Pt/80%Rh, the maximum transport of metals and substantial changes in the wire surface morphology were found to occur in the O_2 atmosphere [9,10]. After annealing in O_2 ($P_{\text{O}_2} \approx 1$ bar) at 1173 K, grain boundaries, facets, etch pits and small crystals were detected for neat Pt and Pt/10 wt.% Rh alloy. For rhodium-containing alloys with an increased Rh content, the enrichment of the alloy surface with rhodium and the appearance of Rh_2O_3 crystals were observed, while for neat Rh—the formation of a continuous Rh_2O_3 oxide layer. The oxidation of PGMs can exert a strong effect on the catalyst etching during NH_3 oxidation.

In our study, Pt(poly), Pd(poly) and Rh(poly) samples were annealed in the O_2 atmosphere at 1100 K, which is close to the temperature of NH_3 oxidation with air oxygen on these samples (ca. 1133 K). For Rh, Pt and Pd, the 1100 K value is close to the Tamman temperature because at this temperature, the T/T_{melt} value for the indicated metals is equal to 0.49, 0.54 and 0.6, which testifies to the high mobility of the metal atoms. As a result, the recrystallization and oxidation of these metals may proceed very intensely. According to Figure 2a, at 1100 K in the O_2 atmosphere, the oxygen concentration on Pt(poly) is equal to ca. 10.0 at.%, on Pd(poly)—to 48.6 at.%, and on Rh(poly)—to 61.1 at.%. On Pt(poly), O atoms are accumulated on such defects as grain boundaries and dislocations; the intercalation of oxygen into the metal lattice was not observed [21]. As a result, the microgranular structure typical of metallic platinum is detected on the Pt(poly) surface. On Pd(poly) and Rh(poly), O atoms both penetrate on defects and intercalate into the lattice of metals. These processes may lead to the formation of particles and/or crystals of PdO and Rh_2O_3 oxides on the surface of Pd and Rh. According to Figure 2b, for the P_{O_2} values

used in this study, at $T = 1100$ K the metallic state of Pt is stable (curve 1). The dependence of equilibrium P_{O_2} above PdO (Figure 2b, curve 2) intersects the value of $P_{O_2} = 1$ bar at $T \sim 1100$ K, which indicates that both the formation and decomposition of PdO solid oxide can occur under such conditions. The reactor temperature may deviate from the maintained value of ca. 1100 K. For Rh, under the given conditions the solid oxide Rh_2O_3 is stable, as shown in Figure 2b, curve 3. These data are consistent with the surface images of the samples annealed in O_2 at 1100 K. For Pt(poly), the microgranular faceted surface typical of recrystallized polycrystalline metals is detected, as shown in Figure S1. For Pd(poly), the cracked and partially decomposed 100–200 nm thick oxide layer consisting of PdO particles and/or crystals with the size of 50–200 nm is observed, as shown in Figure 3a–d. For Rh(poly), a continuous oxide layer of Rh_2O_3 oxide particles with the size of 25–50 nm is formed, in which large 100–200 nm particles and/or crystals of the oxide are seen, as shown in Figure 3e–h. In the O_2 atmosphere (1 bar) at 1100 K, deep oxidation and formation of PdO and Rh_2O_3 oxide layers were revealed for Pd(poly) and Rh(poly), while for Pt(poly) only the microgranular faceted metallic surface was detected without the formation of solid oxides. The penetration of O atoms on Pt(poly) defects and the formation of PdO and Rh_2O_3 solid oxides on Pd(poly) and Rh(poly) may strongly affect the etching of these metals during NH_3 oxidation.

3.2. Catalytic Etching of Pt, Pd and Rh Initiated by the Oxidation of NH_3

High-temperature oxidation of NH_3 gives rise to a deep structural rearrangement of the surface layer in Pt alloy wire of catalytic gauzes (catalytic etching) [3–5,7]. Catalytic etching initiated by NH_3 oxidation forms a rough surface layer comprising etch pits, facets, crystals and large “cauliflowers” on the wire made of neat metals and various alloys [11–13]. In [11–13], the catalyst composition was shown to strongly affect its morphology for neat metals Pt, Rh, Pd, Ag, Ir, Au and alloys Pt/5–40 wt.% Rh, Pt/10–20 wt.% Ir and Pd/5 wt.% Ni that were used in NH_3 oxidation. For all the tested materials, the main reaction zone of NH_3 oxidation with high temperature and a rough etched layer of “cauliflowers” was detected in the central part of the wire. Outside the reaction zone, low-temperature regions having mostly a smooth surface were located. For Pd and Rh outside the main reaction zone, oxide structures represented by the oxide layers as well as “wool”-like and whisker deposits of PdO and Rh_2O_3 were found. For Pt–Rh alloys, a strong effect of Rh concentration on the etching process was revealed, which could be related to the formation of local Rh domains on the Pt surface. Data reported in [11–13,29–31] testify to a strong effect of both the catalyst composition and temperature on the catalyst etching. In addition, the surface structure also affects the etching of Pt catalyst during NH_3 oxidation [29,30].

In our study, after NH_3 oxidation on Pt(poly), Pd(poly) and Rh(poly) at 1133 K for 1, 5 and 10 hours, various etched structures, which formed during the catalytic etching, were detected on the surface. In the process of NH_3 oxidation, the O_2 interaction with metals, particularly the penetration of O atoms on Pt(poly) defects and the formation of PdO and Rh_2O_3 solid oxides on Pd(poly) and Rh(poly), substantially affect the etching of these catalysts. Figure 9 displays images of the most typical fragments of etched layers on Pt(poly) (a,b), Pd(poly) (c,d) and Rh(poly) (e,f) after NH_3 oxidation at 1133 K for 1 h. The images were obtained at high magnifications $\times 100$ k and $\times 300$ k using high-resolution SEM (Regulus 8230). In Figure 9, the capital letters A–F and the arrows indicate the objects discussed in the text.

For Pt(poly), images in Figure 9a,b show the etched structure of the metal surface, which forms during the catalytic oxidation of NH_3 . In Figure 9a,b, one can see regions with hollows (A), which are associated with the segregation of Pt atoms, and pyramidal structures (B), which grow during the catalytic etching. For Pd(poly), images in Figure 9c,d show the etched layer consisting of the metal-oxide fibrous phase, which is formed in the reaction of NH_3 molecules with the PdO oxide-oxygen. Figure 9c,d demonstrates fragments of the fibers with a diameter of 25–50 nm (C) and particles with a size of 5–20 nm (D). Images for Rh(poly) (Figure 9e,f) show the nucleation and growth of the fibrous phase

in the reaction of NH_3 molecules with the oxygen of Rh_2O_3 oxide. Rh_2O_3 oxide particles with the size of 200–300 nm (E) and nuclei of the growing fibrous phase (F) with the size of ca. 50 nm are detected in Figure 9e,f. Such images demonstrate the etched layers that are formed at the very beginning of the etching process. They reveal the morphological features with a size of ca. 3–5 nm, which makes it possible to analyze the mechanism of catalytic etching.

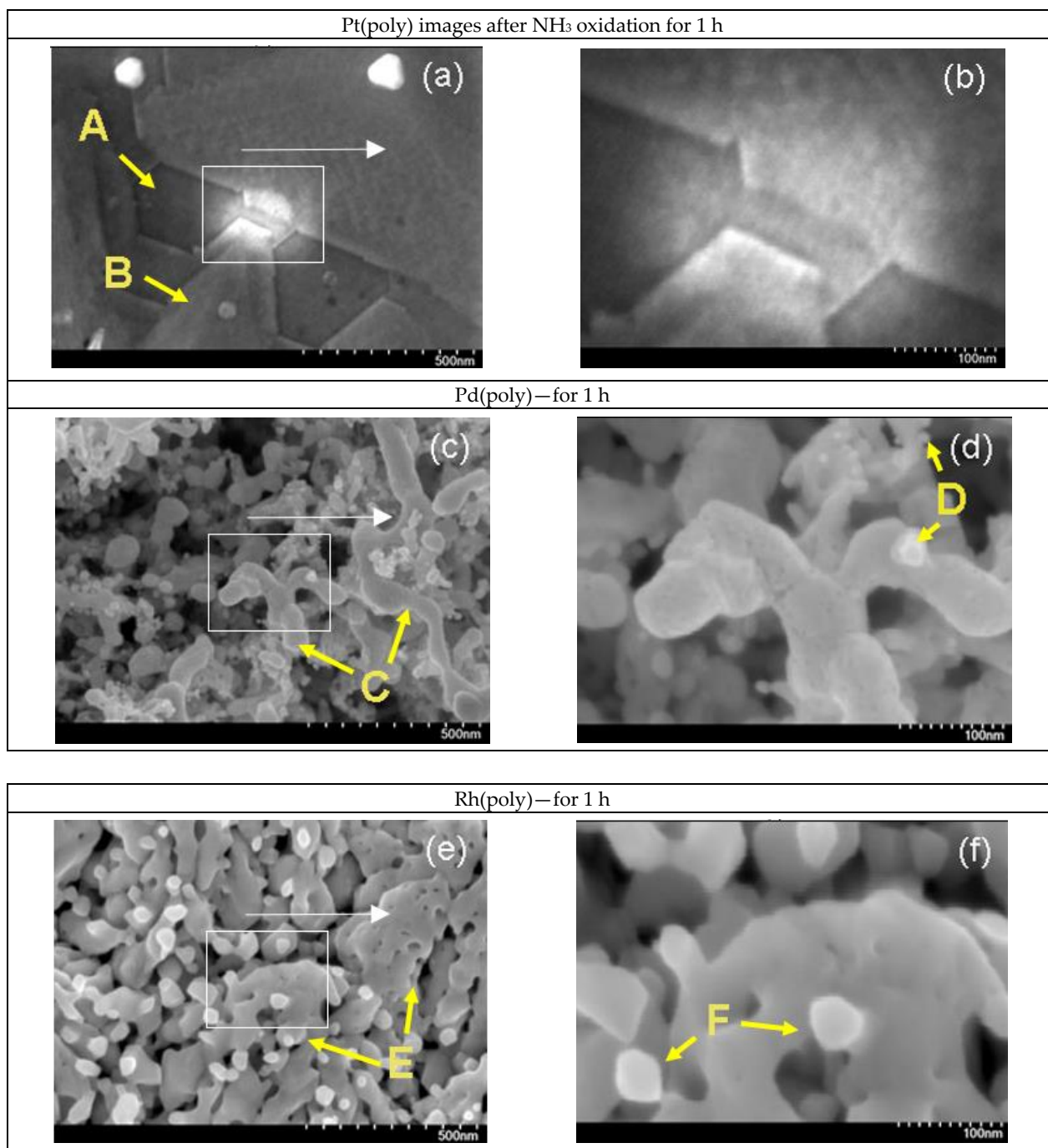


Figure 9. SEM images of the Pt(poly) (a,b), Pd(poly) (c,d) and Rh(poly) (e,f) surface after NH_3 oxidation with air at $T = 1133$ K for 1 h. Images were obtained in SE mode at $E_0 = 5$ keV and $\times 100$ k (a,c,e), $\times 300$ k (b,d,f) magnifications. A–F and arrows indicate the objects discussed in the text. Rectangles indicate the regions represented by images with a higher magnification.

Figure 10a–c indicates the concentrations of metals and C, O, N estimated by EDS on Pt(poly) (a), Pd(poly) (b) and Rh(poly) (c) after NH₃ oxidation for 1, 5 and 10 h. These values were taken from the data of Figures 5 and S2. The concentrations of elements in Figure 10a–c reveal the chemical composition of the etched structures that were formed on these metals upon oxidation of NH₃. Figure 10d–f present models of the catalytic etching initiated by the oxidation of NH₃ at 1133 K for Pt (d), Pd (e) and Rh (f). These models are based on the analysis of images, concentrations of the detected elements and structural characteristics according to SEM, EDS and XRD data obtained for these metals after NH₃ oxidation for 1, 5 and 10 hours. For Pt, Figure 10d shows the O_{ads} and N_{ads} atoms adsorbed on the surface, while O_{ab} and N_{ab} atoms absorbed on defects are indicated in the subsurface region of the metal; in addition, Pt atoms segregating from defects to the surface are also seen. These atoms gradually form crystal facets that are detected on the grain surface. For Rh, Figure 10f displays the Rh₂O₃ oxide layer on the metal surface; O²⁻ and Rh³⁺ ions are indicated in the layer as well as the Rh⁰ atoms segregating to the surface. One can see the pyramidal structures formed during the oxidation of NH₃ on the oxide surface. For Pd, Figure 10e presents the model diagram showing the oxidation of NH₃ and catalytic etching according to different models. At $t = 1$ h—according to the model that is close to that proposed for Rh (Figure 10f), while at $t = 5$ h—according to the model for Pt (Figure 10d).

During the oxidation of NH₃ under the conditions used in this study, stable on Pt(poly) is the metallic state; particles and/or crystals of PtO₂ oxide were not detected on the surface according to SEM, EDS and XRD data. After NH₃ oxidation on Pt(poly) for 1 h, crystal facets of different shapes with a height of up to 0.5–1.0 μm appeared on the surface images, particularly facets with a pyramidal shape and height of 0.1–0.2 μm (Figure 4). After the participation of Pt(poly) in this process for 5 and 10 h, the height of the crystal facets in the images increased up to 1–2 μm. It should be noted that after NH₃ oxidation on the platinum wire for 386 h, terraces 5–10 μm in width and facets ca. 1 μm in height were detected in the low-temperature (<1173 K) region of the wire, while crystal Pt “cauliflowers” with the size of 5–20 μm appeared in the main reaction zone with a high temperature (ca. 1173 K) [11].

According to our XRD data, the fcc lattice parameter a values for new Pt(poly), that after NH₃ oxidation during 10 h and for neat Pt indicated in the PDF database (PDF # 04-0802) are close to each other: 3.920, 3.922 and 3.923 Å, respectively. The concentrations of Pt, C, O and N detected after NH₃ oxidation on Pt(poly) for 1, 5 and 10 h differ insignificantly, as shown in Figure 10a. Pt was detected in a high concentration of 60.7, 56.9 and 62.9 at.%. The concentration of carbon was in the range of 21.0 to 29.3%, oxygen—from 5.7 to 10.9 at.%, and nitrogen—from 4.3 to 6.4 at.%. The detected carbon, oxygen and nitrogen include C_{ab}, O_{ab} and N_{ab} atoms absorbed on defects in the subsurface layers of the catalyst. The above data testify that platinum retains the metallic state for the entire period of NH₃ oxidation. Figure 10d displays the model of NH₃ oxidation and catalytic etching initiated by this reaction for Pt. In the process of NH₃ oxidation on Pt(poly) at 1133 K, O₂ and NH₃ molecules are dissociatively chemisorbed on the surface, while O_{ad} and N_{ad} atoms penetrate on defects and are gradually accumulated in the subsurface region of the catalyst.

The molecules of the NO oxide may form due to the reaction of O_{ad} and N_{ad} atoms chemisorbed on the surface and due to recombination of the dissolved O_{ab} and N_{ab} atoms migrating to the surface. In the course of the reaction between these atoms, a local increase in temperature occurs in the region of defects and “hotspots” are formed; as a result, Pt atoms are segregated to the surface. These processes lead to the formation of etch pits and crystal facets up to 1.0–2.0 μm in height and rearrangement of the Pt(poly) surface, as shown in Figures 4 and 9a,b.

The oxidation of NH₃ on Rh(poly) at 1133 K for 1, 5 and 10 h proceeds on a continuous oxide layer comprising particles and/or crystals of Rh₂O₃ oxide with the size of 0.5–1.0 μm. After NH₃ oxidation for 1 h, fibrous agglomerates are detected on the surface of the oxide layer, as shown in Figure 6a–d. Figure 9e,f display the image of a fragment of such agglomerate consisting of particles/nanocrystals with the size of 25–50 nm. On the surface of the Rh(poly) used in NH₃ oxidation for 5 and 10 h, one can see crystal struc-

tures of the pyramidal shape with sizes equal to 0.3–0.5 μm at the base of the pyramids, 0.05–0.1 μm at the vertex, and a length of ca. 1–2 μm (Figure 6g,h). It should be noted that after NH_3 oxidation on rhodium wire for 23 and 60 h, whiskers and “wool”-like deposits of Rh_2O_3 were detected in the low-temperature (<1173 K) region of the wire [12]. In addition, rhodium “cauliflowers” with a size of 3–80 μm appeared on this wire in the high-temperature (ca. 1173 K) region of the main reaction zone of NH_3 oxidation. The lattice parameter a values for new Rh(poly) that after NH_3 oxidation during 10 h and for neat Rh indicated in the PDF database (PDF # 05-0685) are close to each other: 3.800, 3.800 and 3.803 \AA , respectively. In addition, it should be noted that additional peaks indicating the β - Rh_2O_3 phase were detected on the diffraction pattern for Rh(poly) after NH_3 oxidation, as shown in Figure 8f.

The concentrations of Rh, C, O, N detected on Rh(poly), which was used in the oxidation of NH_3 for 1, 5 and 10 h, differ insignificantly, as shown in Figure 10c. Rh was detected in the concentration of 29.2, 25.9, 28.8 at.%, and oxygen—48.2, 49.0, 51.3 at.%. The concentration of carbon was in the range of 15.0 to 19.2 at.%, and nitrogen—from 4.6 to 5.9 at.%. Carbon (C_{ab}) and nitrogen (N_{ab}) atoms may reside in subsurface layer of the catalyst. SEM, EDS and XRD data evidence that the Rh_2O_3 oxide layer is retained on the Rh(poly) surface for the entire period of NH_3 oxidation. Figure 10f displays the model of NH_3 oxidation on the surface of such oxide layer and formation of the etched structures in the course of the reaction on Rh. This model demonstrates the reaction of NH_3 molecules with oxygen of the Rh_2O_3 oxide layer and the emergence of pyramidal structures. During the oxidation of NH_3 , the produced NO molecules are desorbed into the gas phase, while Rh^0 atoms are segregated to the oxide layer surface. Rh^0 atoms are bound to the oxide much weaker than to the metal, so they can easily migrate over the oxide surface under the given conditions. The migrating Rh^0 atoms and the dissociating Rh_2O_3 oxide gradually form metal-oxide agglomerates of nanofibers and nanocrystals with the size of 25–50 nm and pyramidal crystals with a height up to 1–2 μm (Figures 6 and 9e,f).

At the very beginning of NH_3 oxidation on Pd(poly) ($t = 1$ h), a continuous layer of PdO oxide particles/crystals with a size of 50–200 nm is formed. For a considerable part of this period, the catalyst was held at $T < 1133$ K, which is the temperature at which the PdO oxide is stable, as shown in Figure 2b, curve 2. After the use of Pd(poly) in NH_3 oxidation for 1 h, concentrations of the detected Pd, C, O and N are equal to 51.7, 4.1, 39.2 and 5.0 at.%, respectively, as shown in Figure 10b. These data indicate that the catalyst is in the oxide state at the onset of NH_3 oxidation ($t = 1$ h). As a result, ammonia molecules react predominantly with the oxygen of the oxide layer. The reaction of NH_3 molecules with the oxygen of PdO oxide leads to the release of NO molecules into the gas phase and segregation of Pd^0 atoms to the oxide layer surface; they can form metal-oxide fibrous agglomerates of nanofibers and nanocrystals with the size of 25–50 nm. Figure 9c,d displays the image of a fragment of such agglomerate consisting of nanofibers and nanocrystals with the size of 25–50 nm. In this connection, it can be supposed that at the onset of NH_3 oxidation (at $t = 1$ h), NH_3 molecules are oxidized by the oxygen of PdO oxide according to the model that is close to that proposed for Rh, as shown in Figure 10f. Figure 10e displays the diagram indicating that oxidation of NH_3 and etching of Pd occur at $t = 1$ h according to the model considered for Rh. According to [13], after NH_3 oxidation on palladium wire for 54 h, “wool”-like deposits of PdO and a continuous PdO oxide layer with a thickness of ca. 4 μm were detected in the low-temperature (<1173 K) region of the wire.

In our study, during the long-term oxidation of NH_3 (for 5 h), the Pd(poly) sample was held mostly at $T \sim 1133$ K and even higher temperatures. At $T > 1133$ K and the P_{O_2} value used in the study, stable is the metallic state of palladium, as shown in Figure 2b, curve 2. The obtained lattice parameter a values of the lattice for new Pd(poly) that after NH_3 oxidation during 5 h and for neat Pd indicated in the PDF database (PDF # 46–1043) are close to each other: 3.888, 3.889 and 3.888 \AA , respectively. Taking into account these data and the reaction of NH_3 with the oxygen of the oxide, it can be expected that at this temperature, the PdO oxide particles will rapidly dissociate, while the metallic, palladium

“cauliflowers” will be gradually formed. In [13], palladium “cauliflowers” with the size of 4–55 μm were detected on palladium wire in the region of the main reaction zone of NH_3 oxidation with an increased temperature (ca. 1173 K).

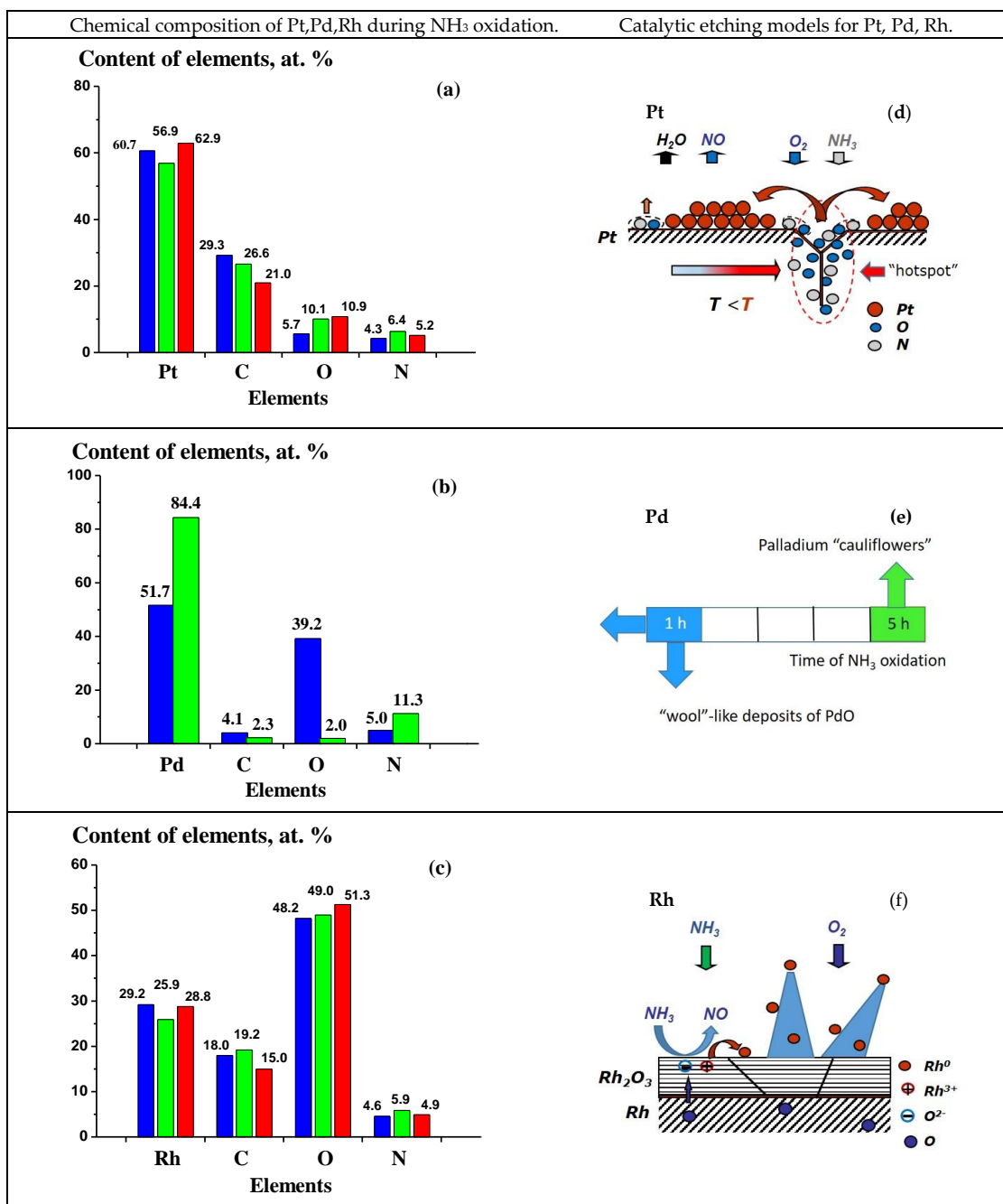


Figure 10. Concentrations of metals (Pt, Pd, Rh) and C, O, N according to EDS data on Pt(poly) (a), Pd(poly) (b) and Rh(poly) (c) after NH_3 oxidation at 1133 K for 1 (left blue columns), 5 (central green columns) and 10 (right red columns) h. Models of NH_3 oxidation and catalytic etching initiated by this reaction for Pt (d), Pd (e) and Rh (f).

The concentrations of Pd, C, O and N detected on Pd(poly) differ significantly after NH_3 oxidation for 1 and 5 h, respectively, as shown in Figure 10b. With an extension of the NH_3 oxidation time from 1 to 5 h, the concentration increases for Pd from 51.7 to 84.4 at.%, and for N—from 5.0 to 11.3 at.%. For oxygen and carbon, a decrease in the concentration from 39.2 to 2.0 at.% for O and from 4.1 to 2.3 at.% for C was observed. These data testify

to the oxide state of the catalyst at the onset of NH_3 oxidation (for 1 h) and the metallic state of palladium in the long-term oxidation of NH_3 (for 5 h). The detected oxygen and nitrogen in the concentration of 2.0 and 11.3 at.% may be associated with the dissolved O_{ab} and N_{ab} atoms in subsurface layers of palladium “cauliflowers”. These data suggest that in the long-term oxidation of NH_3 ($t = 5$ h), NH_3 molecules are oxidized according to the model proposed for Pt, as shown in Figure 10d. The diagram in Figure 10e shows the oxidation of NH_3 and etching of Pd at $t = 5$ h according to the model considered for Pt. During the oxidation of NH_3 on Pd(poly) at 1133 K for 5 h, molecules of NO oxide may form both due to the reaction of adsorbed O_{ad} and N_{ad} atoms on the surface and due to recombination of dissolved O_{ab} and N_{ab} atoms migrating to the surface. These processes lead to the formation of palladium “cauliflowers” with a size of 10–30 μm and rearrangement of the Pd(poly) surface.

It is known that catalytic etching manifests itself in various catalytic systems [26–29]. Such etching strongly affects the essential operating characteristics of catalysts, particularly their activity, mechanical strength, losses of expensive components, etc. In this connection, it is necessary to develop approaches to the analysis of the etching process, including elucidation of the catalytic etching mechanisms and methods of its control. Since etching involves not only the catalyst surface but also its bulk, a possible way for the analysis of this phenomenon is to consider and take into account the reactions that proceed both on the surface and in the subsurface region of the catalyst. The oxidation of NH_3 on PGMs at high T and P can also involve both the O_{ad} and N_{ad} atoms and the N_{ab} and O_{ab} , i.e., it may proceed by the Redox-type mechanism [32]. This mechanism also allows for consideration of the reactions that involve the reagents in the bulk of the catalyst. The quantitative data on the concentration of O_{ab} and N_{ab} in subsurface layers of Pt(poly), Pd(poly) and Rh(poly) obtained in our study may form a basis for modeling with the use of the Redox mechanism of the reactions accompanying the oxidation of NH_3 on PGMs and Pt alloy catalysts.

4. Materials and Methods

The study was carried out using samples of Pt, Pd and Rh polycrystalline foils (Pt(poly), Pd(poly) and Rh(poly)) with the size of $10 \times 5 \times 0.05$ mm, which were obtained by rolling of Pt (GOST 18389-2014), Pd (GOST 18390-2014) and Rh (GOST 19351-2006) rods with the diameter of 6 mm. GOST is the state standard of Russia. According to GOSTs 13498-2010, 13462-2010 and 13098-2006, the Pt, Pd and Rh content in the rods is not lower than 99.9 wt.%, and the content of possible Ir, Ru, Fe, Au, Pb, Si, Sn, Al, Ba and Sb impurities should not exceed 0.07–0.1 wt.%. Particularly, the content of other Pt metals should not be higher than 0.05 wt.%. Before the experiments, surface impurities were removed from the foil samples by treatment in diluted boiling HNO_3 for 30 min with subsequent washing in distilled water. The foil samples were treated in the O_2 atmosphere using a laboratory flow-type quartz reactor with an inner diameter of 14 mm and a volume of 63.6 cm^3 . The samples were mounted parallel to the gas flow in the central part of the reactor at the external surface of a sealed quartz capillary with an outer diameter of 7 mm using a quartz ring. For temperature measurements near the sample in the sealed capillary, a K-type thermocouple was placed close to the sample. The desired temperature of the sample was maintained by a cylindrical electric furnace fitted over the reactor. Samples were treated in an O_2 flow with a weight hourly space velocity of 1.5 L/h at a pressure of ca. 1 bar and temperature 1100 K for 3 h. In addition, Pt(poly) was treated using a gas mixture flow of 21.5 vol.% O_2 in He.

The catalytic oxidation of ammonia with air on Pt(poly), Pd(poly) and Rh(poly) samples were performed in a laboratory flow-type quartz reactor with an inner diameter of 11.2 mm. A ca. 1 mm-thick pack formed by four 3×82 gauzes, which were made of the alloy containing Pt, Pd, Rh and Ru in the concentrations 81, 15, 3.5 and 0.5 wt.%, was placed in the reactor. The foil samples were located before the first gauze, with the side under consideration being arranged against the gas flow. The linear feed rate of the reaction mixture (ca. 10 vol.% NH_3 in the air), which was preheated in a heating mixer to 700 K, was 2.57 m/s; the temperature in the region of gauzes was 1133 ± 5 K; and the total pressure, 3.6 bar. At the indicated pressure

of the ammonia-air mixture and its NH_3 content of 10 vol.%, the pressure of O_2 and NH_3 is 6.8×10^4 and 3.6×10^4 Pa. At these pressures, the O_2 : NH_3 ratio is equal to 1.89. It should be noted that the efficient oxidation of NH_3 to NO requires an excess of O_2 in a mixture with NH_3 compared to the stoichiometric composition (1.25) for the reaction $4\text{NH}_3 + 5\text{O}_2 = 4\text{NO} + 6\text{H}_2\text{O}$. The oxidation of NH_3 to NO is commonly carried out using the ammonia-air mixture with the O_2 : NH_3 ratio in the range of 1.7–2.0 [5]. A detailed description of the employed gauzes and reactor, as well as the conditions of the catalytic process, can be found elsewhere [14–18]. The surface morphology and chemical composition of the subsurface layers of the foil samples were studied using their frontal side relative to the gas flow.

The lattice parameters of the metals were determined on an ARL X'TRA SARK (Thermo Fisher Scientific, Bern, Switzerland) X-ray diffractometer with a $\text{CuK}\alpha$ source ($h\nu = 8048.0$ eV). The surface morphology of the foil samples was investigated using scanning electron microscopes JSM-6460 LV (Jeol, Tokyo, Japan) with a tungsten thermal cathode and Regulus 8230 (Hitachi, Tokyo, Japan) with field emission operated at a probe electron energy (E_0) of 5, 20 and 25 keV. The JSM-6460 LV microscope was equipped with an energy-dispersive X-ray spectrometer INCAx-sight (Oxford Instruments, Abingdon, England, UK), which made it possible to reveal the chemical composition of subsurface layers of the samples. The spectrometer was calibrated using the standards made of neat Si and Co. The quantitative analysis of the chemical composition of samples was performed on an INCA Energy-350 system (Oxford Instruments, Abingdon, England, UK) with the use of internal standards from the spectrometer database. SEM was employed to obtain microimages of the sample surface in the secondary electron (SE) mode with the emission of electrons from the surface layer with a thickness below 5 nm [20]. EDS recorded X-ray quanta of characteristic X-ray radiation with the energy ≤ 10 keV, which are generated in subsurface layers of various materials with a thickness of up to 1 μm [20]. The XRD study was carried out using a $\text{CuK}\alpha$ source with the quantum energy 8048.0 eV; as a result, the depth of analysis for various materials could reach a considerable value, up to 10 μm [21]. Noteworthy is the possibility of using EDS for local chemical analysis with a spatial resolution below 1 μm in the regions presented on micro images. In this study, the local chemical analysis was carried out on the regions with the size from 5×5 to 35×35 μm that were chosen on the surface of samples.

5. Conclusions

SEM, EDS and XRD methods were used to investigate the morphology, chemical composition and structure of Pt(poly), Pd(poly) and Rh(poly) after annealing in the O_2 atmosphere at 1100 K for 3 h and after NH_3 oxidation with air at $T = 1133$ K and a pressure of 3.6 bar for 1, 5 and 10 h. Various etched structures, which formed during the high-temperature annealing in O_2 and NH_3 oxidation with air oxygen, were detected on the surface of these metals at the beginning of the etching process.

After annealing in O_2 and NH_3 oxidation, the microgranular structure of metallic platinum with a grain size of 50–100 μm was observed on Pt(poly). Regular crystal facets were detected on the grain surface; after annealing in O_2 , their height was up to 0.1–0.2 μm , while after the oxidation of NH_3 the height reached 1–2 μm . For the entire period of NH_3 oxidation on Pt(poly), close surface morphology and concentrations of Pt, C, O, N were obtained. According to SEM, EDS and XRD data, under the indicated conditions, platinum was in the metallic state; particles or crystals of PtO_2 oxide were not detected. In the course of the reaction between O_{ab} and N_{ab} atoms migrating to the surface, “hotspots” are formed on the defects; as a result, Pt atoms are segregated to the surface. These processes lead to the formation of etch pits and facets; they can be the nuclei of etched structures on Pt.

On the surface of Rh(poly) a continuous Rh_2O_3 oxide layer was found; after annealing in O_2 , it comprised particles and crystals with the size of 25–50 nm, whereas after NH_3 oxidation—particles with the size of 0.5–1.0 μm . At the beginning of NH_3 oxidation at $t = 1$ h, metal-oxide fibrous agglomerates of nanofibers and nanocrystals with the size of 25–50 nm formed on the oxide layer surface. During the long-term oxidation of NH_3 at

$t = 5\text{--}10$ h, a continuous layer of pyramidal crystals with a length of ca. $1\text{--}2\ \mu\text{m}$ formed on the oxide layer surface. SEM, EDS and XRD data evidence that the Rh_2O_3 oxide layer is retained on the Rh(poly) surface for the entire period of NH_3 oxidation. The reaction of NH_3 molecules with the oxygen of Rh_2O_3 oxide leads to the release of NO molecules into the gas phase and the segregation of Rh^0 atoms to the oxide layer surface. The migrating Rh^0 atoms can form particles/crystals with the size of $25\text{--}50$ nm on the Rh_2O_3 surface, which can serve as the nuclei of metal-oxide nanofibers, nanocrystals and pyramidal crystals forming the etched structures on Rh.

On Pd(poly), a continuous nonuniform oxide layer of PdO particles with the size of $50\text{--}200$ nm was detected after annealing in O_2 , whereas fibrous agglomerates and palladium “cauliflowers” appeared after NH_3 oxidation. At the onset of NH_3 oxidation ($t = 1$ h), fibrous metal-oxide agglomerates of nanofibers and nanocrystals with the size of $25\text{--}50\ \mu\text{m}$ are formed on the oxide layer surface. In the long-term oxidation of NH_3 (for 5 h), a continuous etched layer comprising metallic palladium “cauliflowers” of different shapes and $10\text{--}30\ \mu\text{m}$ size appears on the Pd(poly) surface. According to SEM, EDS and XRD data, the revealed surface morphology, chemical composition and structural characteristics indicate that NH_3 oxidation proceeds on PdO oxide at the onset of the process ($t = 1$ h) and then on metallic palladium ($t = 5$ h). It could be expected that the oxidation of NH_3 and the etching of Pd occur at $t = 1$ h, according to the model considered for Rh, whereas at $t = 5$ h, according to the model considered for Pt.

Supplementary Materials: The following supporting information can be downloaded at: <https://www.mdpi.com/article/10.3390/catal13020249/s1>, Figure S1. SEM images of the Pt(poly) surface after annealing in O_2 at $P_{\text{O}_2} = 1$ bar and 1100 K for 3 h. Images were obtained in SE mode at $E_0 = 20$ keV; rectangles indicate the regions represented by images with a higher magnification.; Figure S2. Concentrations of Pd, C, O and N on Pd(poly) after NH_3 oxidation at 1133 K for 1 (a) and 5 (b) hours according to EDS data obtained at $E_0 = 20$ keV.

Author Contributions: A.S. (Aleksei Salanov): Conceptualization, methodology, writing—original draft, writing—review and editing. A.S. (Alexandra Serkova): Formal analysis, investigation, visualization. L.I.: Conceptualization, resources, validation. S.T.: Formal analysis, investigation. V.P.: Supervision, writing—review and editing. All authors have read and agreed to the published version of the manuscript.

Funding: This work was supported by the Ministry of Science and Higher Education of the Russian Federation within the governmental order for the Boreskov Institute of Catalysis (Project AAAA-A21-121011390053-4).

Acknowledgments: The studies were carried out using the facilities of the shared research center, the National Center of Investigation of Catalysts at the Boreskov Institute of Catalysis.

Conflicts of Interest: The authors declare no conflict of interest.

References

1. International Platinum Group Metals Association (IPA). PGMs in Use. Available online: <http://ipa-news.de/index/pgm-applications> (accessed on 18 November 2022).
2. Matthey, J. PGM Market Reports, May 2021. Available online: <http://www.platinum.matthey.com/services/market-research/pgm-market-reports> (accessed on 18 November 2022).
3. Hatscher, S.T.; Fetzer, T.; Wagner, E.; Kneuper, H. Ammonia Oxidation. In *Handbook of Heterogeneous Catalysis*, 2nd ed.; Ertl, G., Knozinger, H., Schuth, F., Weitkamp, J., Eds.; Wiley-VCH Verlag GmbH & Co. KGaA: Weinheim, Germany, 2008; Volume 5, pp. 2575–2592.
4. Lloyd, L. *Handbook of Industrial Catalysis, Fundamental and Applied Catalysis*; Twigg, M.V., Spencer, M.S., Eds.; Springer Science & Business Media LLC: New York, NY, USA, 2011; pp. 119–131.
5. Karavayev, M.M.; Zasorin, A.P.; Kleshchev, N.F. *Catalytic Oxidation of Ammonia*; Khimia: Moscow, Russia, 1983; pp. 30–122.
6. Handforth, S.L.; Tilley, J.N. Catalysts for Oxidation of Ammonia to Oxides of Nitrogen. *Ind. Eng. Chem.* **1934**, *26*, 1287–1292. [[CrossRef](#)]
7. Ashcroft, J. Optimising Metal Content in Platinum Group Metal Ammonia Oxidation Catalysts. *Johns. Matthey Technol. Rev.* **2021**, *65*, 44–53.

8. Xin, L.; Yongqiang, H.; Husheng, J. Pt-Rh-Pd Alloy Group Gauze Catalysts Used for Ammonia Oxidation. *Rare Met. Mater. Eng.* **2017**, *46*, 339–343. [[CrossRef](#)]
9. Hannevold, L.; Nilsen, O.; Kjekshus, A.; Fjellvag, H. Chemical vapor transport of platinum and rhodium with oxygen as transport agent. *J. Cryst. Growth.* **2005**, *279*, 206–212. [[CrossRef](#)]
10. Hannevold, L.; Nilsen, O.; Kjekshus, A.; Fjellvag, H. Etching of platinum-rhodium alloys in oxygen-containing atmospheres. *J. Alloys Compd.* **2005**, *402*, 53–57. [[CrossRef](#)]
11. Nilsen, O.; Kjekshus, A.; Fjellvag, H. Reconstruction and loss of platinum catalyst during oxidation of ammonia. *Appl. Catal. A Gen.* **2001**, *207*, 43–54. [[CrossRef](#)]
12. Hannevold, L.; Nilsen, O.; Kjekshus, A.; Fjellvag, H. Reconstruction of platinum-rhodium catalysts oxidation of ammonia. *Appl. Catal. A Gen.* **2005**, *284*, 163–176. [[CrossRef](#)]
13. Hannevold, L.; Nilsen, O.; Kjekshus, A.; Fjellvag, H. Surface reconstruction of noble-metal catalysts during oxidation of ammonia. *Appl. Catal. A Gen.* **2005**, *284*, 185–192. [[CrossRef](#)]
14. Salanov, A.N.; Suprun, E.A.; Serkova, A.N.; Sidelnikova, O.N.; Sutormina, E.F.; Isupova, L.A.; Kalinkin, A.V.; Parmon, V.N. Catalytic corrosion of platinum gauzes in the oxidation of ammonia with air. Surface reconstruction of platinum gauzes at 1133 K in air, in ammonia, and in the $\text{NH}_3 + \text{O}_2$ reaction medium. *Kinet. Catal.* **2018**, *59*, 83–98. [[CrossRef](#)]
15. Salanov, A.N.; Suprun, E.A.; Serkova, A.N.; Kochurova, N.M.; Sidel'nikova, O.N.; Sutormina, E.F.; Isupova, L.A.; Kalinkin, A.V.; Parmon, V.N. Catalytic etching of platinum gauzes during the oxidation of ammonia by air. Reconstruction of the surface of a platinum gauze backside in the course of ammonia oxidation at 1133 K. *Kinet. Catal.* **2018**, *59*, 792–809. [[CrossRef](#)]
16. Salanov, A.N.; Suprun, E.A.; Serkova, A.N.; Chesnokova, N.M.; Sutormina, E.F.; Isupova, L.A.; Parmon, V.N. Catalytic etching of platinum gauzes during the oxidation of ammonia by air: Etching of the frontal surface of the platinum gauze in the course of NH_3 oxidation at 1133 K. *Kinet. Catal.* **2020**, *61*, 421–443. [[CrossRef](#)]
17. Salanov, A.N.; Serkova, A.N.; Chesnokova, N.M.; Isupova, L.A.; Parmon, V.N. Characterization of platinum alloy used in ammonia oxidation. Morphology and microstructure of Pt-Pd-Rh-Ru gauzes after the oxidation of NH_3 with air at 1133 K. *Mater. Chem. Phys.* **2021**, *273*, 125138–125151. [[CrossRef](#)]
18. Salanov, A.N.; Chesnokova, N.M.; Serkova, A.N.; Isupova, L.A. Local Chemical Analysis of the Grain Surface, Cauliflowers, and Pores on Pt-Pd-Rh-Ru Gauzes after the oxidation of NH_3 at 1133 K. *Kinet. Catal.* **2021**, *62*, 651–663. [[CrossRef](#)]
19. Salanov, A.N.; Serkova, A.N.; Kalinkin, A.V.; Isupova, L.A.; Parmon, V.N. Chemical composition of the surface and subsurface of Pt-Pd-Rh-Ru catalytic gauzes used in the NH_3 oxidation with air at 1133 K. *Catalysts* **2022**, *12*, 930. [[CrossRef](#)]
20. Goldstein, J.I.; Newbury, D.E.; Michael, J.R.; Ritchie, N.W.M.; Scott, J.H.J.; Joy, D.C. *Scanning Electron Microscopy and X-ray Microanalysis*, 5th ed.; Springer Science & Business Media LLC: New York, NY, USA, 2018; pp. 1–63.
21. Salanov, A.N.; Kochurova, N.M.; Serkova, A.N.; Kalinkin, A.V.; Isupova, L.A.; Parmon, V.N. Oxidation and Recrystallization of Platinum Group Metals (Pt, Pd, Rh) in Oxygen. Surface and Subsurface Reconstruction of Polycrystalline Platinum During Annealing in the O_2 Atmosphere over the Temperature Range of 600–1400 K. *Appl. Surf. Sci.* **2019**, *490*, 188–203. [[CrossRef](#)]
22. Kazenas, E.K.; Chizhikov, D.M. *Vapor Pressure of the Oxides of the Chemical Elements*; Nauka: Moscow, Russia, 1976; pp. 259–273.
23. Fjellvag, A.S.; Waller, D.; Skjelstad, J.; Sjastad, A.O. Grain Reconstruction of Palladium and Palladium-Nickel Alloys for Platinum Catchment. *Johns. Matthey Technol. Rev.* **2019**, *63*, 236–246. [[CrossRef](#)]
24. Ning, Y.; Yang, Z.; Zhao, H. Structure Reconstruction in Palladium Alloy Catchment Gauzes. *Platin. Met. Rev.* **1995**, *39*, 19–26.
25. Ning, Y.; Yang, Z.; Zhao, H. Platinum Recovery by Palladium Alloy Catchment Gauzes in Nitric Acid Plants. *Platin. Met. Rev.* **1996**, *40*, 80–87.
26. Kaichev, V.V.; Teschner, D.; Saraev, A.A.; Kosolobov, S.S.; Gladky, A.Y.; Prosvirin, I.P.; Rudina, N.A.; Ayupov, A.B.; Blume, R.; Hävecke, M.; et al. Evolution of self-sustained kinetic oscillations in the catalytic oxidation of propane over a nickel foil. *J. Catal.* **2016**, *334*, 23–33. [[CrossRef](#)]
27. Bychkov, V.Y.; Tulenin, Y.P.; Slinko, M.M.; Sokolov, S.; Korchak, V.N. Self-Sustained Oscillations as a Method to Increase an Active Surface and Catalytic Activity of Ni and Pd. *Catal. Lett.* **2017**, *147*, 1019–1028. [[CrossRef](#)]
28. Bychkov, V.Y.; Tulenin, Y.P.; Slinko, M.M.; Gorenberg, A.Y.; Shashkin, D.P.; Korchak, V.N. Self-oscillations and surface waves during CO oxidation over Co. *Reac. Kinet. Mech. Cat.* **2019**, *128*, 587–598. [[CrossRef](#)]
29. Flytzani-Stephanopoulos, M.; Schmidt, L.D. Morphology and etching processes on macroscopic metal catalysts. *Prog. Surf. Sci.* **1979**, *9*, 83–111. [[CrossRef](#)]
30. Flytzani-Stephanopoulos, M.; Wong, S.; Schmidt, L.D. Surface Morphology of Platinum Catalysts. *J. Catal.* **1977**, *49*, 51–82. [[CrossRef](#)]
31. Kraehnert, R.; Baerns, M. Morphology changes of Pt-foil catalysts induced by temperature-controlled ammonia oxidation near atmospheric pressure. *Appl. Catal. A Gen.* **2007**, *327*, 73–81. [[CrossRef](#)]
32. Ross, J.R.H. *Contemporary Catalysis, Fundamentals and Current Applications*; Elsevier: Amsterdam, The Netherlands, 2019; pp. 161–173.

Disclaimer/Publisher's Note: The statements, opinions and data contained in all publications are solely those of the individual author(s) and contributor(s) and not of MDPI and/or the editor(s). MDPI and/or the editor(s) disclaim responsibility for any injury to people or property resulting from any ideas, methods, instructions or products referred to in the content.